https://doi.org/10.1016/j.energy.2023.128636

Performance prediction and optimization of cross-flow indirect evaporative cooler by regression model based on response surface methodology

Wenchao Shi [a,*], Hongxing Yang [a], Xiaochen Ma [a], Xiaohua Liu [b,**]

[a] Renewable Energy Research Group (RERG), Department of Building Environment and Energy Engineering, The Hong Kong Polytechnic University, Hong Kong, China

[b] Department of Building Science, Tsinghua University, Beijing, China

Abstract

In recent years, indirect evaporative cooling has rapidly developed with high-accuracy numerical models. As the application of this technology expands from hot-arid areas to hot-humid regions, there is still a lack of regression models of the cross-flow indirect evaporative cooler (IEC) that can be used in different climate regions. Regression models can not only improve prediction efficiency but also be helpful for engineering design. In this study, the regression models of the cross-flow IEC were established based on the response surface methodology (RSM). Eight essential factors, including the inlet air properties, geometric size, and operating parameters, were determined as the input factors, while five indicators were selected as the output responses. The central composite design was employed to generate the matrix for the RSM-based model, and the matrix response data were obtained from an established numerical IEC model validated by the experimental results. The effects of the single and interactive factors are analyzed for each response. Furthermore, the developed models are evaluated by comparing the anticipated results with the on-site measurement data in a real project, and then the multi-objective optimization is conducted for the prediction of IEC performances in five typical cities of China. In summary, the regression models can forecast the cross-flow IEC in a more straightforward approach, which may also assist the design and optimization.

Keywords

Air conditioning; Indirect evaporative cooling; Response surface methodology; Performance prediction; Optimization

Nomenclature

c_{pa}	Specific heat of air, J/(kg · ℃)	*Abbreviation*	
D	Overall desirability score;	ANOVA	Analysis of variance
d	desirability score for each response variable	CCD	Central composite design
f	Input parameter	COP	Coefficient of performance
h	Heat transfer coefficient, W/(m^2 · ℃)	df	Degree of freedom
H	Height, m	IEC	Indirect evaporative cooling
h_{fg}	Heat capacity of vaporization, J/kg	RSM	Response surface methodology
i	Specific enthalpy, kJ/kg	*WF*	Weighting factor

* Corresponding author
** Corresponding author
E-mail addresses:
wenchao511.shi@connect.polyu.hk (W. Shi)
lxh@tsinghua.edu.cn (X. Liu)

l	Lower bound of the response variable	*Greek symbols*	
Le	Lewis number	λ	Thermal conductivity W/(m ·℃)
m	Mass flow rate of air, kg/s	η_{wb}	Wet-bulb efficiency
n	Number of channel pair		
N	Number of parameters		
Nu	Nusselt number	*Subscripts*	
Pr	Prandtl Number	1	Primary air
r	Weight of a corresponding response	2	Secondary air
R^2	Coefficient of determination	c	Condensation
Re	Reynolds number	e	Evaporation
t	Temperature, ℃	i	Inlet
U	Upper bound of the response variable	o	Outlet
v	Velocity, m/s		
w	Humidity ratio, g/kg		
W	Power, W		
y	actual value of the response variable;		
z	Aimed response		
D	Overall desirability score;		

1. Introduction

1.1 Background

Building energy consumption accounts for about 40% of total primary energy usage in developed economies [1]. As many countries strive to achieve carbon peaking and carbon neutrality goals [2], buildings should take responsibility for reducing electricity consumption and greenhouse gas emission. The air conditioning (AC) system maintains thermal comfort for occupants at the cost of around one-third of building energy, and it is necessary to use high-efficient and environmental-friendly air handling approach to mitigate the heavy energy demand. Recently, indirect evaporative cooler (IEC), removing the heat through a physical process without harmful chemical refrigerant, has drawn attention [3-7]. Fig. 1 depicts a plate-type cross-flow IEC system with two airstreams. Water is pumped to the nozzle and diffused to the working air channel to form water membrane, which evaporates because of the humidity gradient when the air is flowing. Then, the middle heat transfer sheet and primary air in the adjacent side are accordingly cooled [8].

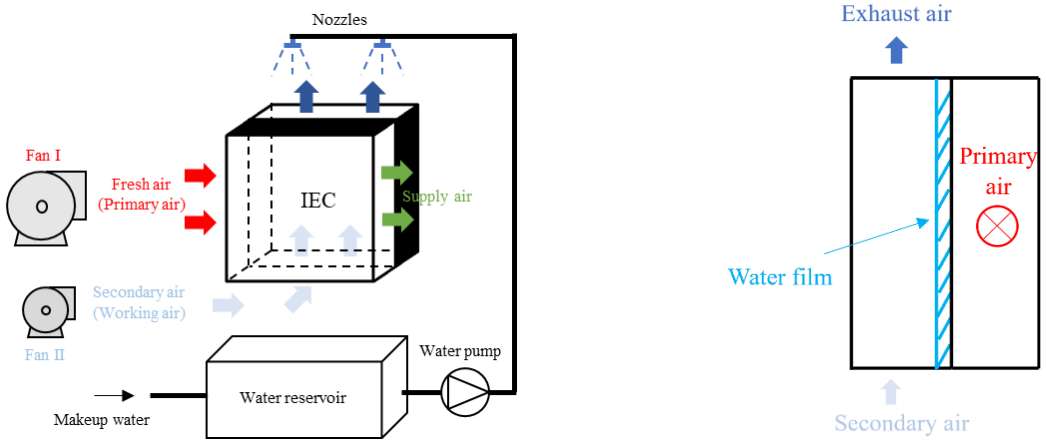

(a) (b)

Fig. 1 (a) A plate-type cross-flow IEC system (b) Left view of the IEC [9]

1.2 Literature review

The models of various types of IECs and hybrid IEC systems have been reported with complete experiments so as to accurately evaluate the cooling performance in the past decade [6, 10-13]. Two-dimensional numerical models were first developed for conventional counter-flow and cross-flow IECs with detailed parameter analysis under steady state [14-16]. Lin et al. further proposed a transient lumped parameter model and a partial differential exergy model to reveal the transient behaviors of a counter-flow IEC [15]. Pandelidis and Anisimov newly established a plate-fin M-cycle model considering the uneven fin temperature and the influence of air mixing [17]. Kabeel and Abdelgaied simulated an IEC with internal baffles and validated the model with experimental data. The increasing number of baffles enhances the cooling performance with the optimal working-to-cooling air ratio of 0.3. Shi et al. constructed a dynamic model for a novel IEC with the porous layer in the working air channel. The periodic spraying was implemented so as to save more energy compared with consistent spraying [18]. Lv et al. proposed an innovative IEC with automatic wetting to save the pump energy,

and they found that the sinusoidal corrugated plate with 45° rotation achieved the best cooling compared with triangular and traditional flat plate IECs [19]. Pacak et al. simulated the variation of air properties and pressure drop of a hexagon IEC using a computational fluid dynamics approach [20]. Zhang et al. numerically studied the hexagon IEC that spraying liquid desiccant in the primary air channel to enhance the dehumidification performance, which improves 16% of the overall performance so as to further expand the application of IEC from conventional hot-arid regions to hot-humid regions [21]. Pandelidis et al. numerically investigated a rotary IEC and compared it with a counter-flow IEC. Results show that rotary IEC had a lower energy demand, a smaller size, and achieved a higher energy efficiency ratio [22]. For the hybrid system, a mathematical model was developed for the system combining a counter-flow IEC, a latent energy system, and a mechanical vapor compression system. High cooling efficiency and load shifting can be realized simultaneously in tropic regions [23]. Wang et al. integrated IEC with a heat pump as a hybrid ventilator and studied the performance in five representative cities, and the system can save 43% energy in temperate regions [9]. Yan et al. assembled the direct expansion system with an IEC considering energy efficiency and indoor air quality, and the fresh air ratio is optimized [24].

Recent theoretical and experimental advancements in indirect evaporative cooling have produced a substantial amount of data, leading to the emergence of statistical models [25-28]. For instance, Min et al. proposed a statistical model to swiftly forecast the cooling performance for the IEC with energy recovery. The empirical equations of wet-bulb efficiency and enlargement coefficient (under condensation state) were accordingly given [29]. However, the decision tree is needed to judge whether condensation would happen before using the equations, which still augments the computation burden. Kiran and Rajput developed the IEC effectiveness model using artificial neural network (ANN), adaptive neuro-fuzzy inference system (ANFIS), and fuzzy inference system (FIS). Results show that the ANN model achieves the best prediction among the three approaches [30]. Shi et al. also proposed an IEC-ANN model, but this model required a large amount of data to ensure acceptable accuracy in the early stage, and the number of hidden layers can greatly influence the modeling establishment speed [31]. Response surface methodology (RSM), a popular statistical approach, has also been used in several evaporative cooling studies. Yan et al. proposed a hollow fiber DEC model and used the simulation data to obtain regression equations of five output responses including outlet air temperature, outlet air relative humidity, saturation effectiveness, cooling capacity, and coefficient of performance (COP) [32]. Sun et al. optimize the wet-bulb efficiency of a tubular IEC considering the effects of six parameters, namely, inlet air temperature, relative humidity, spray water flow rate, secondary-to-primary air ratio, primary air resistance, and secondary air resistance [33]. Pakari and Ghani developed regression models with operational and geometrical parameters for the counter-flow dewpoint IEC system based on the validated numerical model. The outlet air temperature, outlet air relative humidity, and wet-bulb efficiency are determined as the output responses [34].

1.3 Research gaps and contributions of this manuscript

The summary of this study and the previous representative studies is presented in Table 1. Although IEC studies were comprehensively conducted from numerical and experimental perspectives, the following research gaps can still be identified: 1) The regression model of a cross-flow IEC is yet to be developed in different weather conditions; 2) Published models using statistical approaches can

only be adopted in a certain climate zone, which means that one output parameter may have more than one formula in different regions. Using only one equation for one output response to predict the performance under various weather conditions is limited; 3) The optimization of the cross-flow IEC based on the RSM is rarely reported.

To address these research gaps, this study was carried out and structured as follows. Firstly, the experiments and validated numerical models of the cross-flow IEC were first illustrated. Secondly, the regression models of the cross-flow IEC were established based on RSM, which are formulated by the input factors. Thirdly, the effects of single and interactive terms on the output responses were analyzed. Then, the predicted results from the regression models were compared with the data from the real project. Finally, the optimization was conducted for the adjustable factors, and the IEC performances were forecasted in typical Chinese cities with different weather characteristics based on the optimal design.

Table 1 Previous studies of the regression model of evaporative cooling

Research	Type	Approach	Region	Features
Yan et al. [32]	Hollow fiber DEC	RSM	Hot and arid region	Eight input factors and five output responses.
Pakari and Ghani [34]	Counter-flow IEC	RSM	Hot and arid region	Six input factors and three output responses.
Sun et al.[33]	Tubular IEC	RSM	Hot and arid region	Six input factors and one output response.
This study	Cross-flow IEC	RSM	Hot-arid and hot-humid regions	Eight input factors and five output responses

2. Methodology

2.1 Experimental test

Fig. 2 shows the schematic diagram of the experimental test platform, which was established in the underground air-conditioned lab to test the IEC prototype (Fig. 3). The horizontal yellow arrow and vertical blue arrow represent primary air and secondary air, respectively. Air can be heated and humidified by a heater and a humidifier with controllers. Air ducts, the water reservoir, and the prototype are coated with thermal insulation layers. Temperature, relative humidity, and velocity transmitters are equipped on the air ducts, connecting to the data logger with a laptop for recording and monitoring. The timestep is set as one second. The test conditions and geometric parameters of the IEC prototype are listed in Table 2.

Table 2 Test conditions and geometric parameters of the IEC in the experiments

Parameters	Description	Unit	Range
$t_{1,i}$	Primary air inlet temperature	℃	28.20-34.44
$RH_{1,i}$	Primary air relative humidity	%	47.1%-89.7%
v_1	Primary air velocity	m/s	2.01-2.57
$t_{2,i}$	Secondary air inlet temperature	℃	23.02-24.10
$RH_{2,i}$	Secondary air relative humidity	%	59.90-80.74
v_2	Secondary air velocity	m/s	2-2.76
d	Length and width	m	0.4
H	Channel height	m	0.004
n	Channel pair	-	25

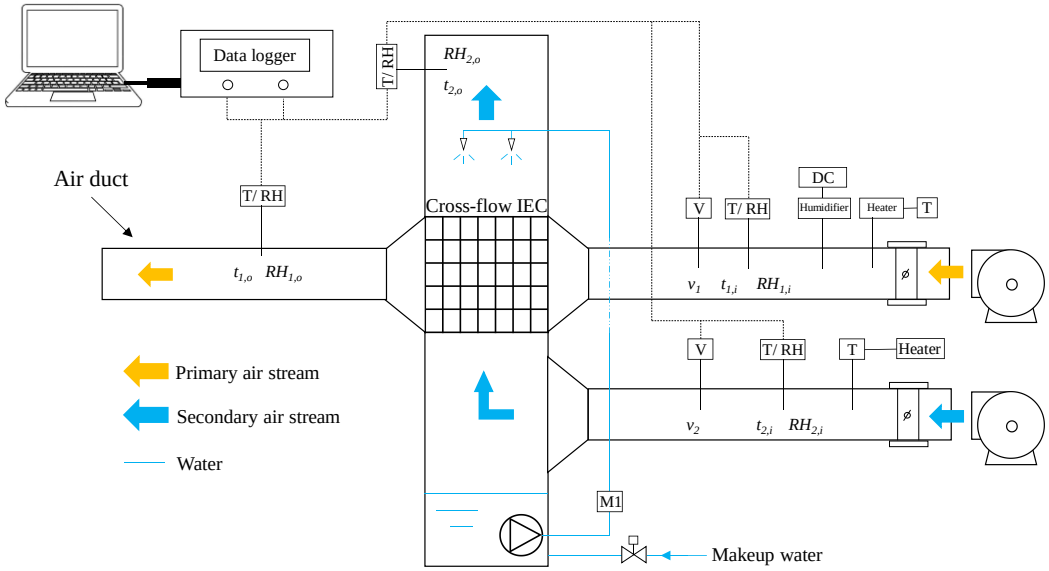

Fig. 2 Schematic diagram of the test platform

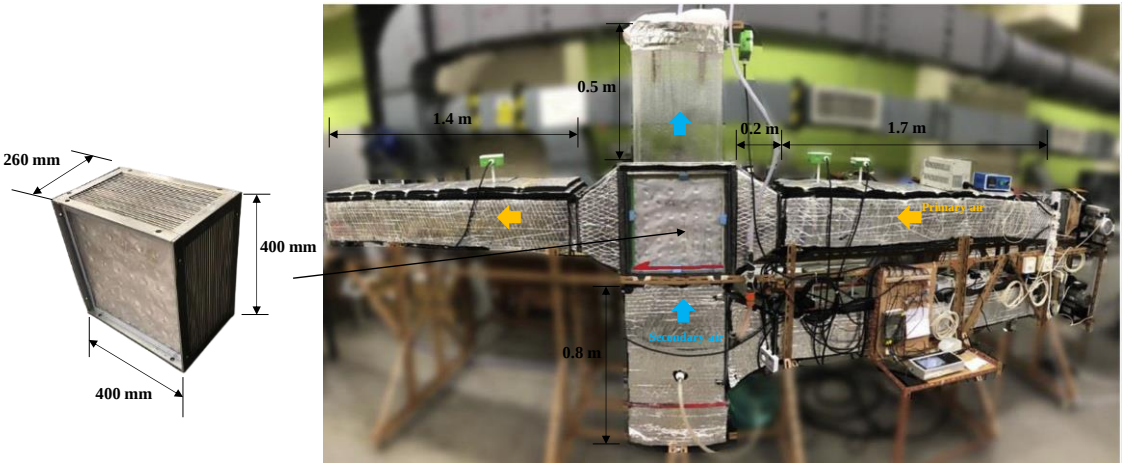

Fig. 3 The IEC prototype and the experimental test platform [35]

2.2 Numerical model

When the primary air is hot and arid, the heat transfer process can be written is:

$$h_1(t_1 - t_w) \cdot dxdy = c_{pa}\dot{m}_1 \frac{\partial t_1}{\partial y} dx \tag{1}$$

$$\dot{m}_1 = \frac{dy}{H} m_1 \tag{2}$$

In the secondary air channel, the evaporation is mainly driven by the humidity gradient between water film and air, and the process is expressed by Eq. (3) and Eq. (4). To obtain a higher cooling performance, exhaust air from the air-conditioned area is used as the secondary air in this study, which has a lower and stable wet-bulb temperature.

$$h_{fg}h_{m2}(\omega_{t_w} - \omega_2)dxdy + h_2(t_w - t_2) \cdot dxdy = \dot{m}_2 \frac{\partial i_2}{\partial y} dy \tag{3}$$

$$h_{m2}(\omega_{t_w} - \omega_2) \cdot dxdy = m_2 \frac{\partial \omega_2}{\partial y} \cdot dy \tag{4}$$

$$\dot{m}_2 = \frac{dx}{L} m_2 \tag{5}$$

The energy balance in the IEC is formulated as:

$$\dot{m}_2 \frac{\partial i_2}{\partial y} - c_{pa}\dot{m}_1 \frac{\partial t_1}{\partial x} = c_{pw}t_{ew} \frac{\partial m_e}{\partial y} \tag{6}$$

$$\frac{\partial m_e}{\partial y} = \dot{m}_s \frac{\partial w_2}{\partial y} \tag{7}$$

If the primary air is hot and moist, such as in the Guangdong Province of China, sensible and latent cooling may coincide. The mass equation of the moisture content should be added (Eq. (8)). Besides, the energy balance equation is revised as Eq. (10).

$$h_{m1}(\omega_{t_w} - \omega_1) \cdot dxdy = \dot{m}_1 \frac{\partial \omega_1}{\partial x} \cdot dx \tag{8}$$

$$-\dot{m}_1 \frac{\partial \omega_1}{\partial x} = \frac{\partial m_c}{\partial y} \tag{9}$$

$$\dot{m}_2 \frac{\partial i_2}{\partial y} - \dot{m}_1 \frac{\partial i_1}{\partial x} = c_{pw}t_{ew} \frac{\partial (m_e)}{\partial y} + c_{pw}t_{cw} \frac{\partial (m_c)}{\partial y} \tag{10}$$

The Nusselt number is necessary when the heat transfer coefficient is calculated, and the Lewis number connects the convective heat and mass transfer coefficients, which are written from Eq. (11) to Eq. (13).

$$Nu_* = 0.664 Re_*^{\frac{1}{2}} Pr_*^{\frac{1}{3}} \tag{11}$$

$$h_* = \frac{Nu_* \cdot \lambda}{d_e} \tag{12}$$

$$Le^{\frac{2}{3}} = \frac{h_*}{h_{m*} c_{pa}} \tag{13}$$

where *=1, 2.

The boundary conditions of the numerical model have been listed in our previous study [36], which is not repeated here to make the content concise and avoid duplication.

2.3 RSM-based regression model

RSM uses multiple quadratic terms to fit the functional relationship between input factors and the response in many events. The form can be expressed by Eq. (14). According to the input factors and output responses, the central composite design (CCD) is employed to organize the events, which is based on the 2-level factorial designs improved with center and axial points for fitting quadratic models [37]. Each factor usually has five levels from low to high values in CCD. In this study, eight essential parameters are used as input factors. Their ranges and values in five grades are given in Table 3. Besides, the five output responses are determined for conducting RSM, namely, wet-bulb efficiency (η_{wb}), enlargement coefficient (ε), outlet temperature ($t_{1,o}$), outlet humidity ratio ($w_{1,o}$), and *COP*, which are more concerned in the published IEC studies [2, 38, 39]. The equations for calculating wet-bulb efficiency (η_{wb}), enlargement coefficient (ε), and *COP* are written from Eq. (15) to Eq. (17).

$$z = b_0 + \sum_{a=1}^{n} \beta_a f_a + \sum_{a=1}^{n} \sum_{a<b}^{n} \beta_{ab} f_a f_b + \sum_{a=1}^{n} \beta_{aa} f_a^2 + c_0 \tag{14}$$

where: y – the aimed response; f_a, f_b - the input parameters; N - the number of parameters (8 in this study); b_0 - intercept coefficient; β_a, β_{ab}, β_{aa} - coefficient of the linear, interactive, and quadratic item; c_0 - experiment errors.

$$\eta_{wb} = \frac{t_{1,i} - t_{1,o}}{t_{1,i} - t_{wb2,i}} \tag{15}$$

$$\varepsilon = \frac{m_1 c_{pa}(t_{1,i} - t_{1,o}) + m_1(w_{1,i} - w_{1,o}) h_{fg}}{m_1 c_{pa}(t_{1,i} - t_{1,o})} \tag{16}$$

$$COP = \frac{Q}{W} \tag{17}$$

Table 3 The parameters, ranges, and corresponding levels in the central composite design

Parameters	Unit	Levels in ascending order				
$t_{1,i}$	℃	20	25	30	35	40
$RH_{1,i}$	%	30	47.5	65	82.5	100
v_1	m/s	0.5	1.25	2	2.75	3.5
$t_{2,i}$	℃	20	21.75	23.5	25.25	27

$RH_{2,i}$	%	0.4	0.5	0.6	0.7	0.8
v_2	m/s	0.5	1.25	2	2.75	3.5
d	m	0.004	0.00475	0.0055	0.00675	0.007
H	m	0.4	0.8	1.2	1.6	2

After determining the input factors and output responses, the CCD matrix containing eight input factors and five output responses can be generated using the Design Expert software. The analysis of variance (ANOVA) is carried out for the model of the selected responses. The significance is evaluated by comparing the p-value with a bound of 0.05. Each term with a p-value lower than 0.05 is considered significant, while the items with p-values higher than 0.05 are insignificant [40].

3. Results and discussion

3.1 Numerical model validation

The results produced by the numerical model are compared with the data obtained from the experiments in section 2.1 for validation. The same geometric and operating parameters are used in both the experiments and the numerical simulations. The experimental data under non-condensation and condensation states are plotted in Fig. 4, which match well with the simulation values. It can be observed that the deviations are within 2% under the non-condensation state. Under the condensation state, the discrepancies of primary air outlet temperature and humidity are within 5% and 6.5%, respectively. These deviations are slightly larger than those under the non-condensation state but are still within a reasonable range. Therefore, it can be demonstrated that the numerical model is able to accurately predict the performance of the cross-flow IEC under both non-condensation and condensation states.

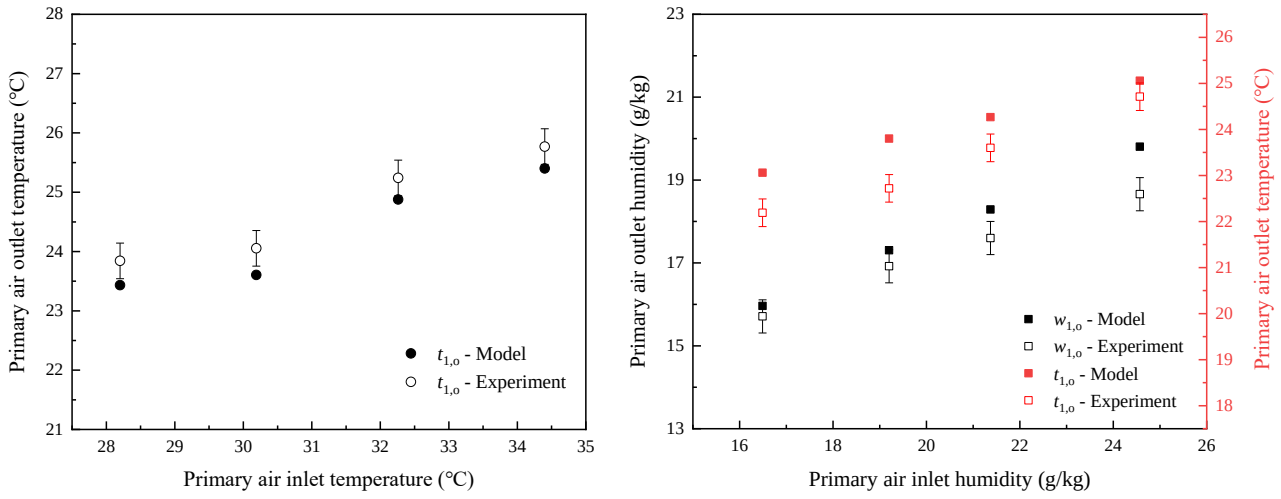

(a) (b)

Fig. 4 Validation of the numerical model under (a) non-condensation state and (b) condensation state

3.2 Regression analysis

The events in the CCD matrix are processed by the validated IEC model, and the results based on the 282 groups of input factors are written in Supplementary Material as well. Referring to the design

matrix, the ANOVA is conducted for the five responses, and the fit statistics results are presented in Table 4. It can be seen that all responses modeled in the quadratic form are significant as their p-value are tiny and lower than 0.05. The coefficients of determination (R^2) are close to 1, which means that the fitting quality is satisfactory. The comparisons between actual and predicted responses are shown in Fig. 5, and the plotted points locate around the line segment with a slope of 1, echoing the results of R^2. Furthermore, the adequate precision and the difference between the adjusted R^2 and predicted R^2 are checked. The adequate precisions of the five output responses are substantially larger than 4, and the difference between the adjusted R^2 and predicted R^2 for each response is much less than 0.2, which meets the modeling requirements [41, 42].

Table 4 Fit statistics results of the selected responses

Response	Source	p-value	R^2	Adj.R^2	Pred.R^2	Adj.R^2 -Pred.R^2	Adequate precision
η_{wb}	Quadratic	<0.0001	0.9728	0.9678	0.9597	0.0081	81.7
ε	Quadratic	<0.0001	0.9790	0.9751	0.9692	0.0059	85.3
$t_{1,o}$	Quadratic	<0.0001	0.9896	0.9877	0.9848	0.0029	126.6
$w_{1,o}$	Quadratic	<0.0001	0.9870	0.9845	0.9818	0.0027	106.3
COP	Quadratic	<0.0001	0.9899	0.9881	0.9838	0.0043	112.1

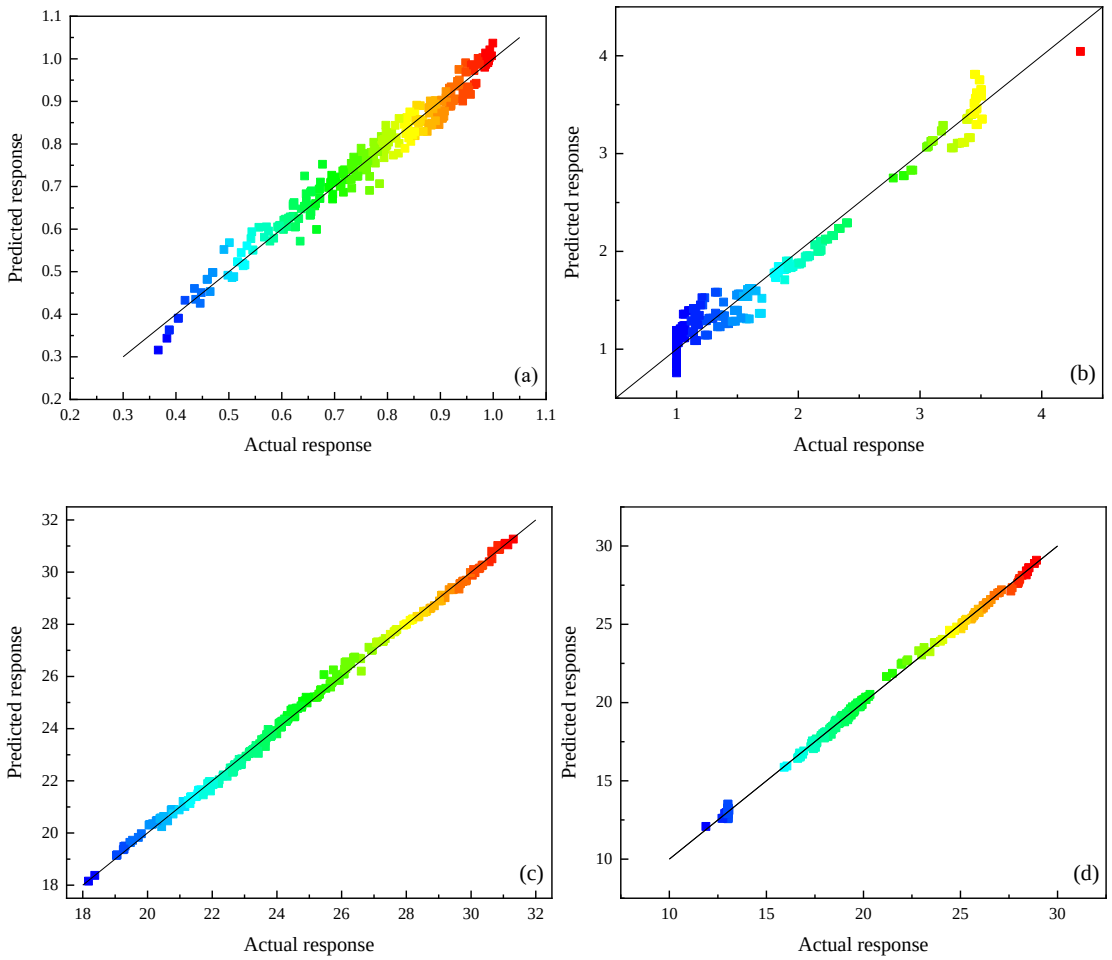

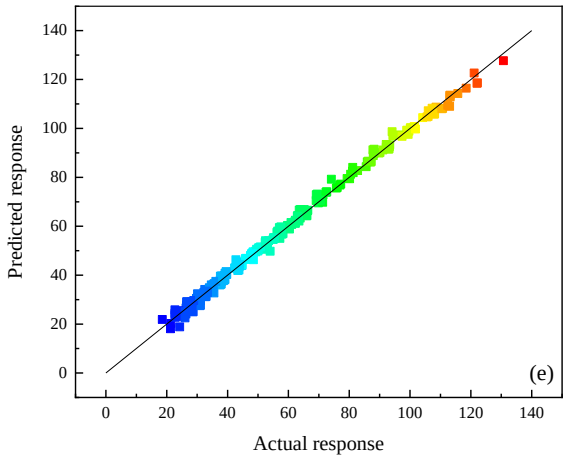

Fig. 5 Comparison between the predicted result and the actual value of (a) η_{wb} (b) ε (c) $t_{1,o}$ (d) $w_{1,o}$ (e) *COP*

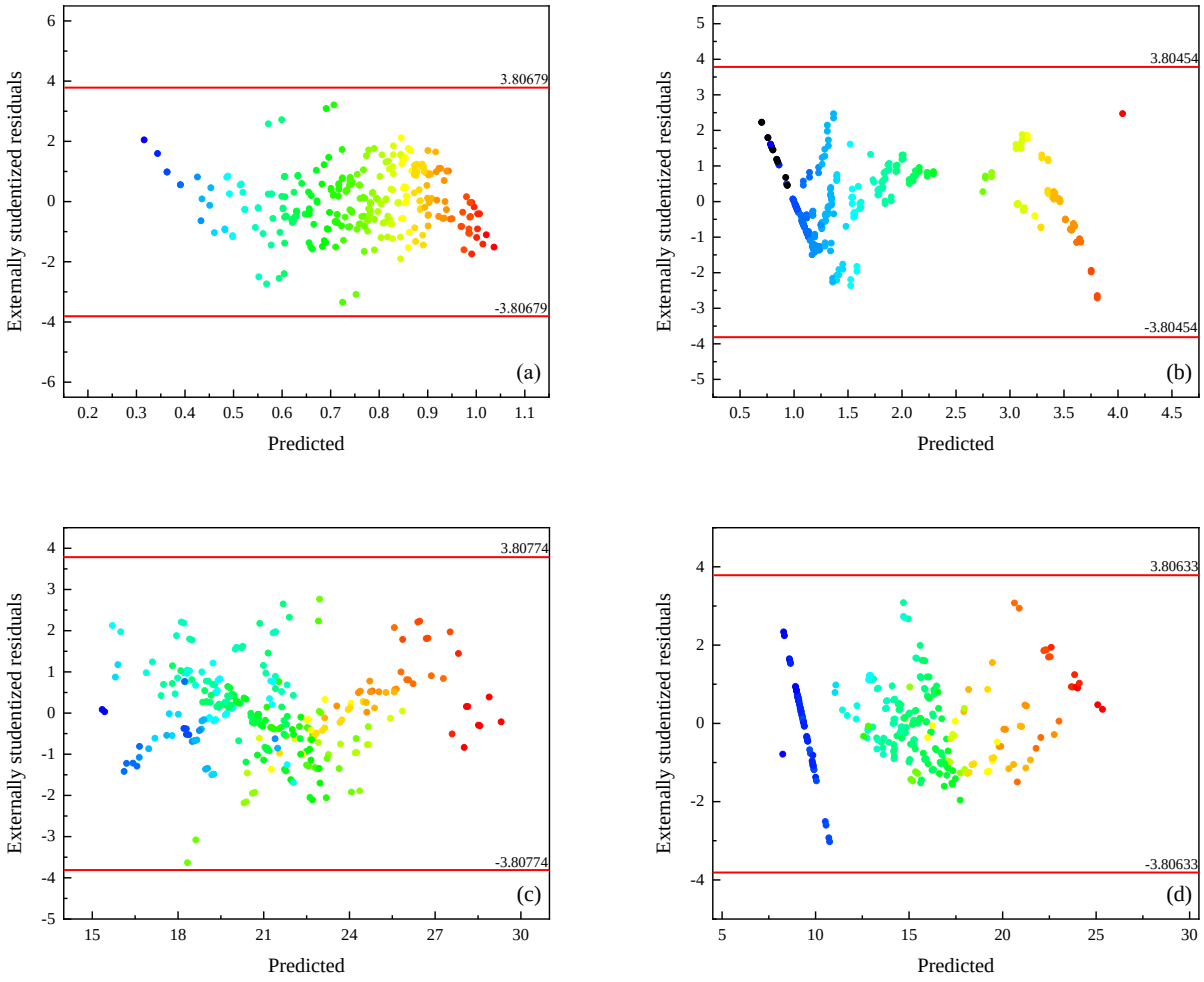

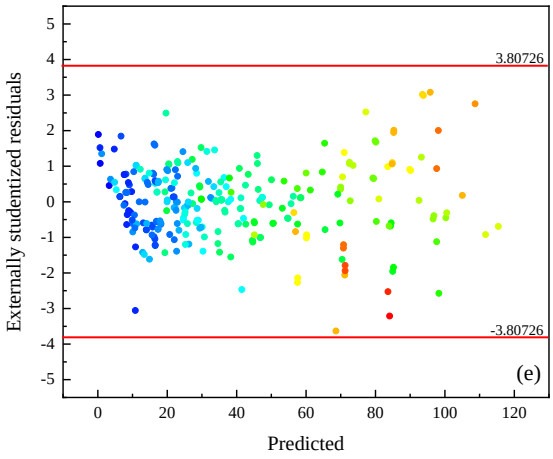

Fig. 6 Distribution of the externally studentized residuals of (a) η_{wb} (b) ε (c) $t_{1,o}$ (d) $w_{1,o}$ (e) *COP*

In addition to the ANOVA and fit statistics, the distributions of externally studentized residuals against the predicted values of each response, as a visual check for the assumption of constant variance [41], are plotted in Fig. 6. It can be seen that all points casually scatter with no regulations, and the points locate in the range of residuals within the red line, which means that the original observations are irrelevant with the response results [32]. Therefore, the regression models can cautiously predict the performance of the cross-flow IEC.

3.3 Output Responses

The results of the five output responses are reported from the perspectives of the regression model, perturbation plot, and the response surface. The regression model is obtained after conducting the ANOVA, and the effect of a single input factor on the tendency and sensitivity can be summarized from the perturbation plot. Then, the response surface is presented to reveal the influence of the significant interactive factors that can be artificially influenced, namely primary air velocity, secondary air velocity, channel height, and the length of the IEC for this study. Thus, the four factors can form six interactive pairs (v_1~v_2, v_1~d, v_1~H, v_2~d, v_2~H, d~H). Akaike's Information Criterion (AIC), which can seek for a model that can interpret data with the least number of parameters, is employed for model correction. Therefore, some pairs may be removed from the six pairs. This section only discusses the interactive factor pairs that meet the criterion. In addition, if the p-value of a term is greater than 0.05, this term is excluded as well.

3.3.1 Wet-bulb efficiency

The results of ANOVA for the response of wet-bulb efficiency are shown in Table 5. The total sum of squares is 6.22 with 6.05 attributed to the model and 0.17 attributed to the residual. The model and residual have degrees of freedom of 31 and 250, respectively. More importantly, we have removed 10 out of 28 interactive terms and 3 out of 8 square terms by AIC. It can be noticed that all linear terms are significant, while an interactive term (dH- channel height and IEC height/length) and a square term (t_2^2) are insignificant. Hence, the two can be removed from the regression model. The regression model of this response is formulated in Eq. (18).

Table 5 ANOVA for the response of the wet-bulb efficiency

Source	Sum of squares	df	Mean square	F-value	p-value	Judgment
Model	6.05	31	0.1950	283.92	< 0.0001	++
Linear						
$t_{1,i}$	0.3412	1	0.3412	496.68	< 0.0001	++
$RH_{1,i}$	1.47	1	1.47	2140.16	< 0.0001	++
v_1	2.06	1	2.06	3004.11	< 0.0001	++
$t_{2,i}$	0.1080	1	0.1080	157.17	< 0.0001	++
$RH_{2,i}$	0.0980	1	0.0980	142.71	< 0.0001	++
v_2	0.8293	1	0.8293	1207.36	< 0.0001	++
d	0.0313	1	0.0313	45.57	< 0.0001	++
H	0.8000	1	0.8000	1164.68	< 0.0001	++
Interactive						
t_1RH_1	0.0752	1	0.0752	109.47	< 0.0001	++
t_1v_1	0.0041	1	0.0041	5.91	0.0158	+
t_1t_2	0.0039	1	0.0039	5.75	0.0173	+
t_1RH_2	0.0028	1	0.0028	4.12	0.0435	+
t_1v_2	0.0065	1	0.0065	9.49	0.0023	+
RH_1v_1	0.0537	1	0.0537	78.22	< 0.0001	++
RH_1t_2	0.0064	1	0.0064	9.39	0.0024	+
RH_1RH_2	0.0070	1	0.0070	10.14	0.0016	+
RH_1v_2	0.0562	1	0.0562	81.89	< 0.0001	++
v_1t_2	0.0043	1	0.0043	6.22	0.0133	+
v_1RH_2	0.0045	1	0.0045	6.54	0.0111	+
v_1v_2	0.0149	1	0.0149	21.68	< 0.0001	++
v_1H	0.0066	1	0.0066	9.55	0.0022	+
t_2RH_2	0.0083	1	0.0083	12.15	0.0006	++
t_2v_2	0.0037	1	0.0037	5.40	0.0209	+
RH_2v_2	0.0040	1	0.0040	5.76	0.0171	+
v_2H	0.0030	1	0.0030	4.43	0.0363	+
dH	0.0022	1	0.0022	3.17	0.0760	-
Square						
RH_1^2	0.0032	1	0.0032	4.67	0.0317	+
v_1^2	0.0067	1	0.0067	9.78	0.0020	+
t_2^2	0.0017	1	0.0017	2.44	0.1196	-

v_2^2	0.0099	1	0.0099	14.39	0.0002	+
H^2	0.0139	1	0.0139	20.27	< 0.0001	++
Residual	0.1717	250	0.0007			
Lack of Fit	0.1717	241	0.0007			
Pure Error	0.0000	9	0.0000			
Cor Total	6.22	281				

++: Extremely significant (p-value<0.001); +: Significant (0.001<p-value<0.05); -: Insignificant (p-value>0.05)

$$\eta_{wb} = 0.763878 + 0.0195076t_1 - 0.0465098RH_1 - 0.271562v_1 - 0.00563988t_2 - 0.575328RH_2 + 0.130785v_2 - 14.5187d + 0.361644H - 0.0195863t_1RH_1 - 0.00106146t_1v_1 - 0.000448746t_1t_2 - 0.0066491t_1RH_2 + 0.00134586t_1v_1 - 0.110379RH_1v_1 + 0.0163897RH_1t_2 + 0.298125RH_1RH_2 + 0.112933RH_1v_2 + 0.00311269v_1t_2 + 0.055874v_1RH_2 + 0.0135585v_1v_2 + 0.016869v_1H + 0.0326315t_2RH_2 - 0.00289993t_2v_2 - 0.0524366RH_2v_2 + 0.0114903v_2H - 0.278038RH_1{}^2 + 0.0258102v_1{}^2 - 0.0277832v_2^2 - 0.116976H^2 \quad (18)$$

The perturbation plot can reflect the influence of the input factors on the tendency and sensitivity of the response. The positive gradient of a curve means that the value of an output response grows with the increasing input factor, while the negative gradient indicates that the higher value of a factor leads to a reduction of the response. In addition, the response is more sensitive to a factor when the curve gradient is steep. The perturbation plot of the wet-bulb efficiency is presented in Fig. 7. The actual factors are given as well, which are the input conditions used for the perturbation plots of the other four output responses. It is seen that the primary air velocity (v_1) has the most inverse impact on the growth of wet-bulb efficiency, while the higher secondary air velocity (v_2) and the IEC height (H) both have the most positive effect on larger response values. It needs to be mentioned that the influences of some factors such as primary air inlet temperature ($t_{1,i}$) and secondary air relative humidity ($RH_{2,i}$) seem different from some studies. The reason is that this perturbation plot is based on the actual factors that lead to condensation. The response value decreases when the amount of condensation increases. On the contrary, the greater RH_2 causes the wet-bulb temperature of the secondary air to be higher than the dew point temperature of the primary air, thereby gradually transforming into a process dominated by sensible heat transfer so as to increase the wet-bulb efficiency.

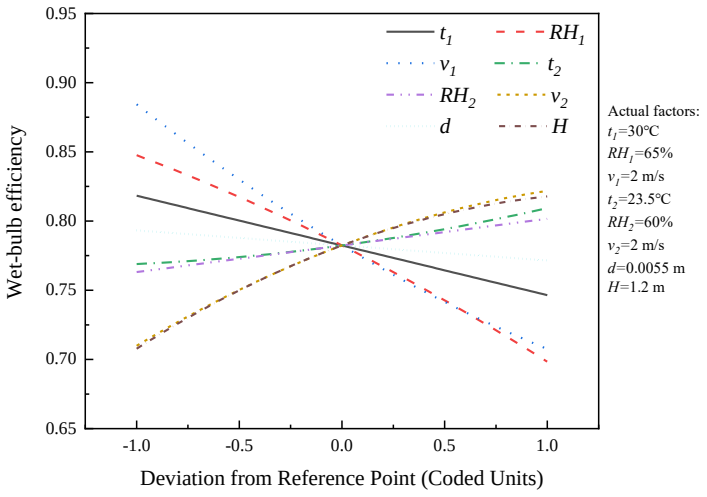

Fig. 7 Perturbation plot of the wet-bulb efficiency

After analysis of the single factors, the response surfaces and contours are shown in Fig. 8 to show the influence of the interactive factors. When the interactive terms vary in their ranges, the other six input factors are set at their mean values of the five levels [32]. For the response of wet-bulb efficiency, only three interactive terms (v_1~v_2, v_1~H, and v_2~H) satisfy the AIC and the requirement of the p-value. It is found from Fig. 8(a) that the highest value of 1.05 can be obtained by decreasing primary air velocity (v_1) and increasing secondary air velocity (v_2) simultaneously. Besides, the surfaces and contours of v_1~H and v_2~H from Fig. 8(b)-(c) indicate that the taller heat exchanger is recommended with larger v_1 and lower v_2.

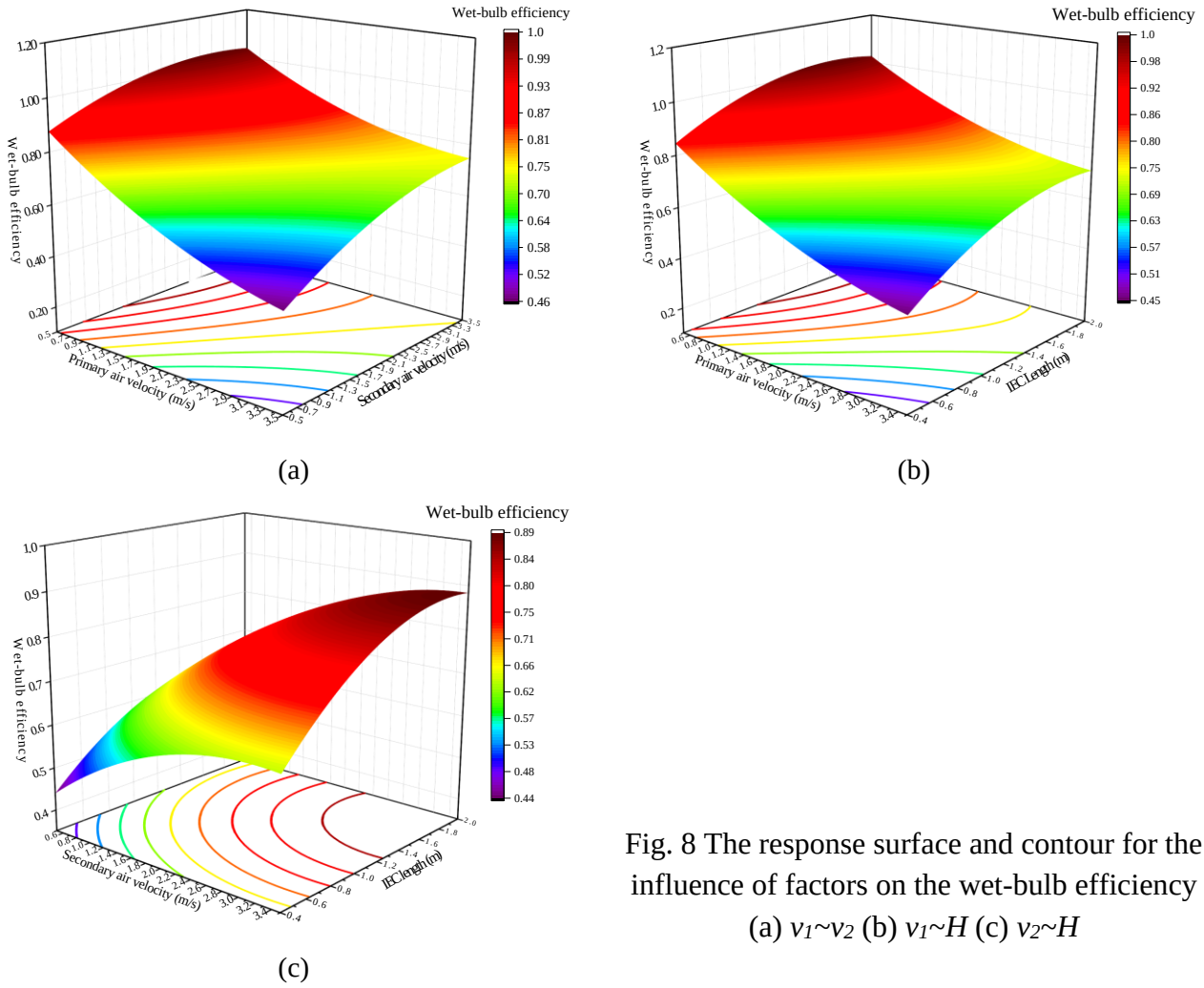

Fig. 8 The response surface and contour for the influence of factors on the wet-bulb efficiency (a) v_1~v_2 (b) v_1~H (c) v_2~H

3.3.2 Enlargement coefficient

The ANOVA for the response of the enlargement coefficient is shown in Table 6. The total sum of squares is 239.65, consisting of 234.54 from the model and 5.11 from the residual. The values of the degree of freedom are 21 and 260 for the model and residual, respectively. The p-values of the eight linear terms are lower than 0.05, demonstrating their significance. However, 17 out of 28 interactive pairs and 5 out of 8 square terms are removed because of the AIC. Besides, the p-values of t_1v_2 and v_2^2 exceed the upper bound so as to be regarded as insignificant items. Thus, the two are not

included in the regression model of the response as well. Then, the regression model of the enlargement coefficient can be formulated as Eq. (19) based on the remaining source in Table 6.

Table 6 ANOVA for the response of the enlargement coefficient

Source	Sum of squares	df	Mean square	F-value	p-value	Judgment
Model	234.54	21	11.17	567.97	< 0.0001	++
Linear						
$t_{1,i}$	54.98	1	54.98	2796.24	< 0.0001	++
$RH_{1,i}$	136.46	1	136.46	6939.90	< 0.0001	++
v_1	1.92	1	1.92	97.59	< 0.0001	++
$t_{2,i}$	2.65	1	2.65	134.53	< 0.0001	++
$RH_{2,i}$	2.46	1	2.46	125.30	< 0.0001	++
v_2	1.22	1	1.22	62.17	< 0.0001	++
H	0.2145	1	0.2145	10.91	0.0011	+
Interactive						
$t_{1,i}RH_{1,i}$	28.35	1	28.35	1441.89	< 0.0001	++
$t_{1,i}v_1$	0.0814	1	0.0814	4.14	0.0429	+
$t_{1,i}t_{2,i}$	0.2573	1	0.2573	13.09	0.0004	+
$t_{1,i}RH_{2,i}$	0.2501	1	0.2501	12.72	0.0004	+
$t_{1,i}v_2$	0.0572	1	0.0572	2.91	0.0894	-
$RH_{1,i}v_1$	0.3958	1	0.3958	20.13	< 0.0001	++
$RH_{1,i}t_{2,i}$	0.5929	1	0.5929	30.15	< 0.0001	++
$RH_{1,i}RH_{2,i}$	0.5553	1	0.5553	28.24	< 0.0001	++
$RH_{1,i}v_2$	0.3231	1	0.3231	16.43	< 0.0001	++
v_1v_2	0.1389	1	0.1389	7.06	0.0084	+
$t_{2,i}RH_{2,i}$	0.3070	1	0.3070	15.61	0.0001	++
Square						
$t_{1,i}^2$	0.2093	1	0.2093	10.64	0.0013	+
$RH_{1,i}^2$	2.68	1	2.68	136.34	< 0.0001	++
v_2^2	0.0563	1	0.0563	2.86	0.0919	-
Residual	5.11	260	0.0197			
Lack of Fit	5.11	251	0.0204			
Pure Error	0.0000	9	0.0000			
Cor Total	239.65	281				

++: Extremely significant (p-value<0.001); +: Significant (0.001<p-value<0.05); -: Insignificant (p-value>0.05)

$$\varepsilon = 8.72011 - 0.431394t_{1,i} - 12.9823RH_{1,i} + 0.140919v_1 + 0.054964t_{2,i} + 3.53877RH_{2,i} - 0.16803v_2 + 0.0712636H + 0.380339t_{1,i}RH_{1,i} - 0.00475559t_{1,i}v_1 + 0.00362341t_{1,i}t_{2,i} + 0.0625071t_{1,i}RH_{2,i} - 0.299599RH_{1,i}v_1 - 0.157139RH_{1,i}t_{2,i} - 2.66149RH_{1,i}RH_{2,i} + 0.270693RH_{1,i}v_2 + 0.0414058v_1v_2 - 0.197876t_{2,i}RH_{2,i} + 0.00270509t_{1,i}^2 + 8.48303RH_{1,i}^2 \quad (19)$$

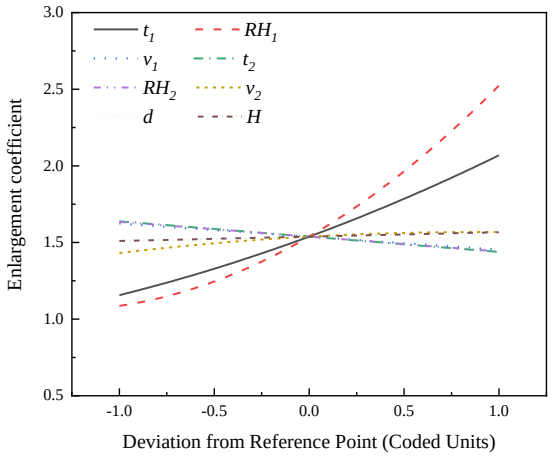

Fig. 9 Perturbation plot of the enlargement coefficient

Regarding the variation trend of the eight single factors, it can be seen from Fig. 9 that the growing primary air inlet temperature ($t_{1,i}$) and relative humidity ($RH_{1,i}$) are positive to increase the value of the response, and the curve of RH has an increasing slope. The slopes of secondary air velocity (v_2), channel height (d), and IEC height (H) are flat compared with the former two, indicating that the sensitivity of the three single factors is not intensive. The greater values of secondary air temperature ($t_{2,i}$), $RH_{2,i}$, and primary air velocity (v_1) lead to the opposite tendency of the enlargement coefficient with similar sensitivity.

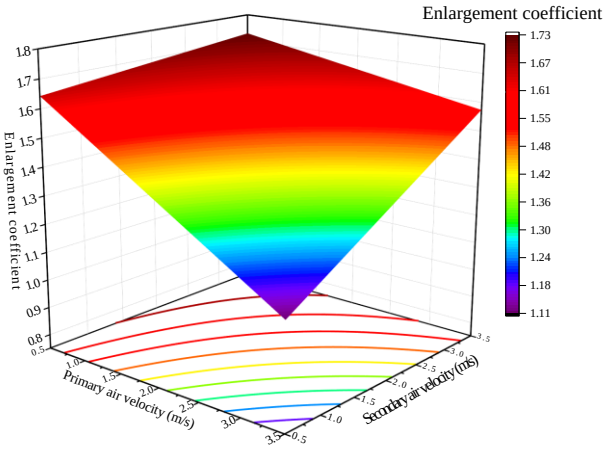

Fig. 10 The response surface and contour for the influence of v_1~v_2 on the enlargement coefficient

Fig. 10 presents the response surface and contour plots for the enlargement coefficient. Only one interactive term (v_1v_2) stays after AIC and p-value checking. The enlargement coefficient can be generally enhanced by reducing the primary air velocity (v_1) and increasing the secondary airspeed (v_2) simultaneously, which shares the same approach with the response of wet-bulb efficiency. The peak point on the response surface occurs when v_1 and v_2 are 0.5 m/s and 3.5 m/s, respectively,

corresponding to the maximum value of 1.73.

3.3.3 Outlet temperature of primary air

Table 7 ANOVA for the response of the outlet temperature of primary air lists the results of ANOVA for the response of the outlet temperature of primary air. The total sum of squares is 2217.26, consisting of 2193.78 from the model and 23.47 from the residual. The values of the degree of freedom are 35 and 246 for the model and residual, respectively. All linear terms are significant and will occur in the regression model as their p-values are lower than 0.05. 22 interactive and 5 square items satisfy the AIC. The number of remaining interactive terms of this response is the most among the other four. However, the p-values of two interactive (v_1H, dH) and one square source ($RH_{1,i}^2$) go beyond the upper limit of the p-value, which are excluded from the final model of this response. Thus, the regression model of the outlet temperature of primary air is written by Eq. (20).

In respect to the effect of the single factor on the response tendency, as presented in Fig. 11, the growing primary air inlet temperature ($t_{1,i}$), relative humidity ($RH_{1,i}$), and velocity (v_1) and secondary air inlet temperature ($t_{2,i}$) and relative humidity ($RH_{2,i}$) of cause the higher primary air outlet temperature. Enlarging the channel height is also positive to the response value, but this factor is less sensitive than the former five. The negative slopes of secondary air velocity (v_2) and channel height (d) indicate that the output value is reduced when the two factors are bigger.

Table 7 ANOVA for the response of the outlet temperature of primary air

Source	Sum of squares	Df	Mean square	F-value	p-value	Judgment
Model	2193.78	35	62.68	656.94	< 0.0001	++
Linear						
$t_{1,i}$	693.34	1	693.34	7266.86	< 0.0001	++
$RH_{1,i}$	253.63	1	253.63	2658.23	< 0.0001	++
v_1	305.85	1	305.85	3205.55	< 0.0001	++
$t_{2,i}$	230.92	1	230.92	2420.23	< 0.0001	++
$RH_{2,i}$	214.71	1	214.71	2250.34	< 0.0001	++
v_2	128.69	1	128.69	1348.77	< 0.0001	++
H	4.28	1	4.28	44.87	< 0.0001	++
$t_{1,i}$	109.43	1	109.43	1146.97	< 0.0001	++
Interactive						
$t_{1,i}RH_{1,i}$	75.06	1	75.06	786.71	< 0.0001	++
$t_{1,i}v_1$	60.43	1	60.43	633.35	< 0.0001	++
$t_{1,i}t_{2,i}$	3.18	1	3.18	33.34	< 0.0001	++
$t_{1,i}RH_{2,i}$	3.23	1	3.23	33.84	< 0.0001	++
$t_{1,i}v_2$	28.47	1	28.47	298.36	< 0.0001	++
$t_{1,i}d$	0.6654	1	0.6654	6.97	0.0088	+

$t_{1,i}H$	16.44	1	16.44	172.29	< 0.0001	++
$RH_{1,i}v_1$	12.15	1	12.15	127.31	< 0.0001	++
$RH_{1,i}t_2$	3.06	1	3.06	32.11	< 0.0001	++
$RH_{1,i}RH_{2,i}$	3.03	1	3.03	31.80	< 0.0001	++
$RH_{1,i}v_2$	11.02	1	11.02	115.54	< 0.0001	++
$v_1t_{2,i}$	7.70	1	7.70	80.68	< 0.0001	++
$v_1RH_{2,i}$	7.35	1	7.35	77.07	< 0.0001	++
v_1 v_2	1.21	1	1.21	12.73	0.0004	+
v_1H	0.3581	1	0.3581	3.75	0.0539	-
$t_{2,i}RH_{2,i}$	0.9653	1	0.9653	10.12	0.0017	+
$t_{2,i}v_2$	3.75	1	3.75	39.30	< 0.0001	++
$t_{2,i}H$	1.81	1	1.81	18.93	< 0.0001	++
$RH_{2,i}v_2$	3.65	1	3.65	38.23	< 0.0001	++
$RH_{2,i}H$	1.66	1	1.66	17.41	< 0.0001	++
v_2H	0.7747	1	0.7747	8.12	0.0047	+
dH	0.2699	1	0.2699	2.83	0.0939	-
Square						
$t_{1,i}^2$	1.00	1	1.00	10.52	0.0013	+
$RH_{1,i}^2$	0.3257	1	0.3257	3.41	0.0659	-
v_1^2	1.13	1	1.13	11.83	0.0007	+
v_2^2	1.16	1	1.16	12.11	0.0006	+
H^2	1.67	1	1.67	17.55	< 0.0001	++
Residual	23.47	246	0.0954			
Lack of Fit	23.47	237	0.0990			
Pure Error	0.0000	9	0.0000			
Cor Total	2217.26	281				

++: Extremely significant (p-value<0.001); +: Significant (0.001<p-value<0.05); -: Insignificant (p-value>0.05)

$$t_{1,o} = -4.25846 - 0.0775268t_1 - 0.994263RH_1 + 2.34218v_1 + 0.874112t_2 + 10.4747RH_2 - 1.25147v_2 - 238.074d - 4.88295H + 0.618842t_1RH_1 + 0.12956t1v_1 - 0.0127402t_1t_2 - 0.224617t_1RH_2 - 0.0889234t_1v_2 + 13.5955t_1d - 0.126699t_1H + 1.65963RH_1v_1 - 0.357225RH_1t_2 - 6.22073RH_1RH_2 - 1.58109RH_1v_2 - 0.132116v_1t_2 - 2.25972v_1RH_2 - 0.122459v_1v_2 + 0.350884t_2RH_2 + 0.0922085t_2v_2 + 0.120002t_2H + 1.59145RH_2v_2 + 2.01357RH_2H - 0.183372v_2H + 0.00715919{t_1}^2 - 0.291787{v_1}^2 + 0.339793{v_2}^2 + 1.42204H^2 \quad (20)$$

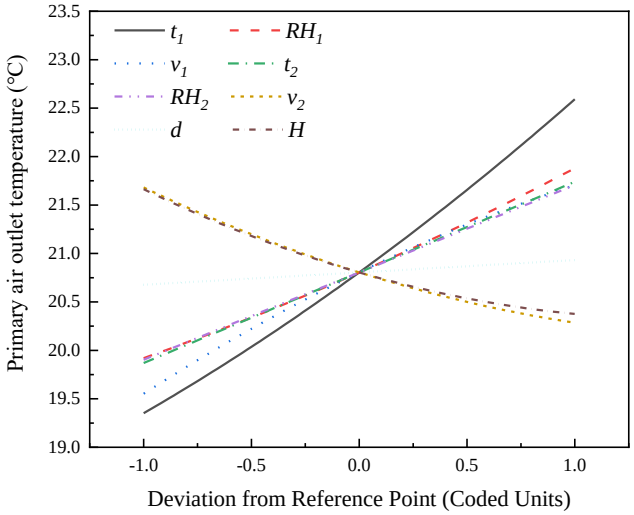

Fig. 11 Perturbation plot of the outlet temperature of primary air

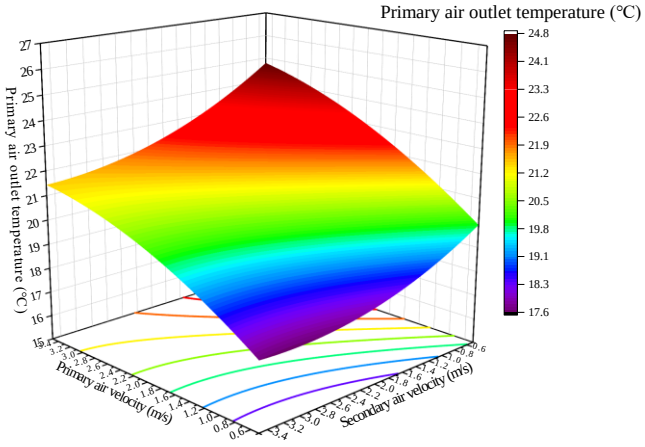

(a)

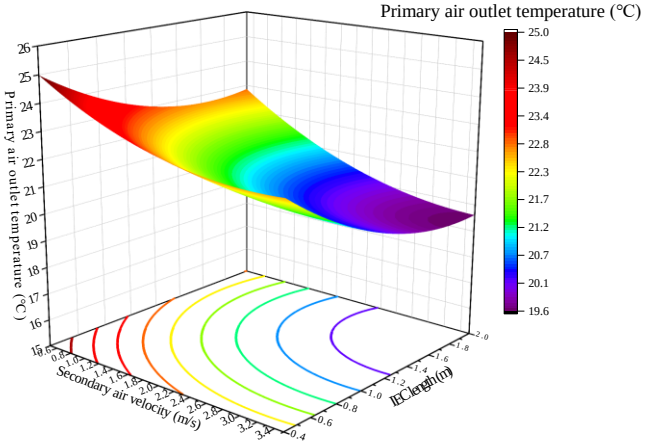

(b)

Fig. 12 The response surface and contour for the influence of factors on the outlet temperature of primary air (a) v_1~v_2 (b) v_2~H

Regarding the adjustable interactive terms, two of them (v_1v_2, v_2H) pass the AIC and p-value checking. Therefore, their response surface and contours are present in

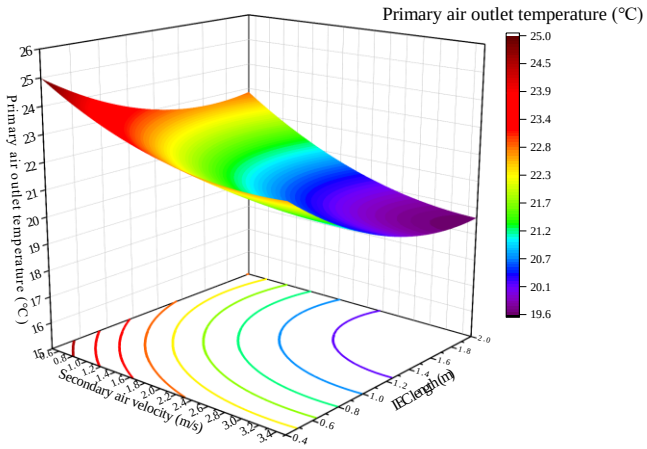

(b)

Fig. 12. It is noticed that the lower temperature results from the tardy primary air speed (v_1), faster secondary air velocity (v_2), and extended channel height (d). The minimum temperatures are 19.6℃ and 17.6℃ when v_1= 0.5 m/s, v_2= 3.11 m/s and v_2= 3.5 m/s H= 1.85 m, respectively.

3.3.4 Outlet humidity ratio of primary air

The results of ANOVA for the response of the primary air outlet humidity are presented in Table 8. The model has a sum of squares of 4404.58 and a degree of freedom of 29. In addition, all linear terms are significant and used to establish the regression model. Among the interactive and square terms, 20 interactive and only 1 square item pass the AIC. In addition, it can be noticed from the table that the p-values of four interactive sources exceed 0.05, which are not included in the final model of this response. Therefore, the regression model of the primary air outlet humidity ratio is written by Eq. (21).

Table 8 ANOVA for the response of the outlet humidity ratio of primary air

Source	Sum of squares	df	Mean square	F-value	p-value	Judgment
Model	4404.58	29	151.88	624.08	< 0.0001	++
Linear						
$t_{1,i}$	1972.36	1	1972.36	8104.46	< 0.0001	++
$RH_{1,i}$	1557.34	1	1557.34	6399.13	< 0.0001	++
v_1	190.25	1	190.25	781.74	< 0.0001	++
$t_{2,i}$	87.56	1	87.56	359.77	< 0.0001	++
$RH_{2,i}$	80.64	1	80.64	331.35	< 0.0001	++
v_2	98.59	1	98.59	405.11	< 0.0001	++
H	1.46	1	1.46	5.99	0.0151	+
$t_{1,i}$	38.28	1	38.28	157.29	< 0.0001	++
Interactive						
$t_{1,i}RH_{1,i}$	15.10	1	15.10	62.03	< 0.0001	++

$t_{1,i}v_1$	92.17	1	92.17	378.72	< 0.0001	++
$t_{1,i}t_{2,i}$	9.40	1	9.40	38.64	< 0.0001	++
$t_{1,i}RH_{2,i}$	8.42	1	8.42	34.58	< 0.0001	++
$t_{1,i}v_2$	47.07	1	47.07	193.40	< 0.0001	++
$t_{1,i}d$	0.7153	1	0.7153	2.94	0.0877	-
$t_{1,i}H$	18.69	1	18.69	76.82	< 0.0001	++
$RH_{1,i}v_1$	73.80	1	73.80	303.26	< 0.0001	++
$RH_{1,i}t_{2,i}$	14.98	1	14.98	61.55	< 0.0001	++
$RH_{1,i}RH_{2,i}$	13.61	1	13.61	55.94	< 0.0001	++
$RH_{1,i}v_2$	40.91	1	40.91	168.10	< 0.0001	++
$RH_{1,i}$ H	11.45	1	11.45	47.06	< 0.0001	++
$v_1t_{2,i}$	5.14	1	5.14	21.13	< 0.0001	++
$v_1RH_{2,i}$	4.90	1	4.90	20.15	< 0.0001	++
v_1H	0.7830	1	0.7830	3.22	0.0741	-
$t_{2,i}v_2$	2.70	1	2.70	11.09	0.0010	+
$t_{2,i}H$	0.9344	1	0.9344	3.84	0.0512	-
$RH_{2,i}v_2$	2.62	1	2.62	10.77	0.0012	+
$RH_{2,i}H$	0.8519	1	0.8519	3.50	0.0625	-
v_2H	1.27	1	1.27	5.22	0.0232	+
Square						
$RH_{1,i}^2$	12.58	1	12.58	51.70	< 0.0001	++
Residual	8.56	248	0.0345			
Lack of Fit	8.56	239	0.0358			
Pure Error	0.0000	9	0.0000			
Cor Total	4814.98	281				

++: Extremely significant (p-value<0.001); +: Significant (0.001<p-value<0.05); -: Insignificant (p-value>0.05)

$$w_{1,o} = -0.759453 + 0.0655246t_1 + 20.8299RH_1 - 2.68273v_1 - 0.781925t_2 - 12.9252RH_2 + 2.22936v_2 + 99.0653d + 5.53509H - 0.277518t_1RH_1 + 0.160007t_1v_1 + 0.0219048t_1t_2 + 0.362623t_1RH_2 - 0.114341t_1v_2 - 0.135116t_1H + 4.09089RH_1v_1 + 0.789832RH_1t_2 + 13.1775RH_1RH_2 - 3.04573RH_1v_2 - 3.02146RH_1H - 0.107979v_1t_2 - 1.84528v_1RH_2 + 0.078214t_2v_2 + 1.34922RH_2v_2 - 0.234803v_2H - 18.1213RH_1^2 \quad (21)$$

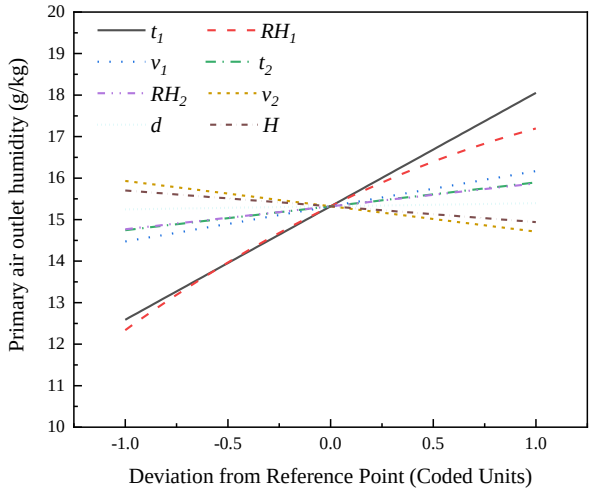

Fig. 13 Perturbation plot of the outlet humidity ratio of primary air

The perturbation plot in Fig. 13 shows the influence of the single factors on the variation trend of the response. It can be observed that the higher secondary air velocity (v_2) and IEC height (H) can decrease the response value, and the latter is more sensitive because of the steeper slope. On the other hand, the other six factors have the opposite impact, and response grows as these factors increase.

For the response surface and contour, only one interactive term (v_2H) satisfies the AIC and p-value checking. As shown in Fig. 14, the reduction of the response can be realized by increasing the secondary air velocity (v_2) and adding the IEC height (H) concurrently, and the minimum value on the response surface is found as 13.06 g/kg when v_2 and H are 3.5 m/s and 2 m, respectively.

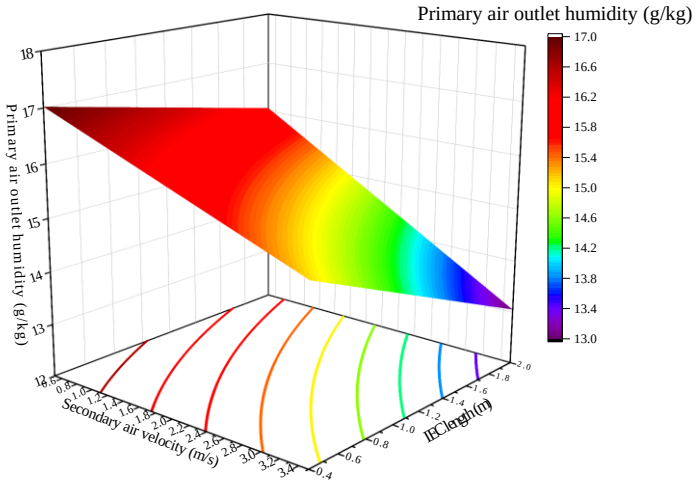

Fig. 14 The response surface and contour for the influence of v_2~H on the outlet humidity ratio of primary air

3.3.5 COP

Table 9 displays the ANOVA results for the response of *COP*. The total sum of squares is 2.10×10^5 with 2.079×10^5attributed to the model and 2173.78 attributed to the residual. The values of degree of freedom are 33 and 248 for the model and residual, respectively. More importantly, seven linear

terms are significant except the IEC height (H) due to the high p-value of 0.1261. It is the only response that not all linear terms are used in the regression model formulation. However, it is a non-hierarchical model if the basic single factor is removed, and the predictions are unlikely to match the actual model predictions [41]. Thus, this single term is reserved just to ensure the model is a hierarchical model. 20 interactive and 5 square terms meet the AIC. However, one interactive term (RH_1v_1) has a p-value of 0.1018, which exceeds the upper bound of the p-value, and it needs to be removed from the model of *COP*. Hence, the form of the regression model is presented in Eq. (22).

Table 9 ANOVA for the response of the *COP*

Source	Sum of squares	df	Mean square	F-value	p-value	Judgment
Model	2.079E+05	33	6298.55	718.58	< 0.0001	++
Linear						
$t_{1,i}$	1.191E+05	1	1.191E+05	13588.04	< 0.0001	++
$RH_{1,i}$	35907.05	1	35907.05	4096.53	< 0.0001	++
v_1	3388.77	1	3388.77	386.62	< 0.0001	++
$t_{2,i}$	7121.42	1	7121.42	812.46	< 0.0001	++
$RH_{2,i}$	6970.77	1	6970.77	795.28	< 0.0001	++
v_2	7891.13	1	7891.13	900.28	< 0.0001	++
D	3246.93	1	3246.93	370.43	< 0.0001	++
H	20.65	1	20.65	2.36	0.1261	-
Interactive						
$t_{1,i}RH_{1,i}$	16842.38	1	16842.38	1921.50	< 0.0001	++
$t_{1,i}v_1$	571.73	1	571.73	65.23	< 0.0001	++
$t_{1,i}t_{2,i}$	100.35	1	100.35	11.45	0.0008	+
$t_{1,i}RH_{2,i}$	108.80	1	108.80	12.41	0.0005	+
$t_{1,i}v_2$	1832.56	1	1832.56	209.07	< 0.0001	++
t_1G	937.03	1	937.03	106.90	< 0.0001	++
$RH_{1,i}v_1$	23.64	1	23.64	2.70	0.1018	-
$RH_{1,i}t_{2,i}$	297.36	1	297.36	33.93	< 0.0001	++
$RH_{1,i}RH_{2,i}$	287.56	1	287.56	32.81	< 0.0001	++
$RH_{1,i}v_2$	50.33	1	50.33	5.74	0.0173	+
$RH_{1,i}d$	294.22	1	294.22	33.57	< 0.0001	++
v_1v_2	857.11	1	857.11	97.79	< 0.0001	++
v_1d	43.79	1	43.79	5.00	0.0263	+
$t_{2,i}RH_{2,i}$	34.33	1	34.33	3.92	0.0489	+
$t_{2,i}v_2$	85.90	1	85.90	9.80	0.0020	+

$t_{2,i}d$	53.07	1	53.07	6.05	0.0146	+
$RH_{2,i}v_2$	67.15	1	67.15	7.66	0.0061	+
$RH_{2,i}d$	51.33	1	51.33	5.86	0.0162	+
v_2H	164.47	1	164.47	18.76	< 0.0001	++
dH	146.44	1	146.44	16.71	< 0.0001	++
Square						
$t_{1,i}^2$	707.37	1	707.37	80.70	< 0.0001	++
$RH_{1,i}^2$	428.53	1	428.53	48.89	< 0.0001	++
v_1^2	188.58	1	188.58	21.51	< 0.0001	++
v_2^2	57.67	1	57.67	6.58	0.0109	+
H^2	51.10	1	51.10	5.83	0.0165	+
Residual	2173.78	248	8.77			
Lack of Fit	2173.78	239	9.10			
Pure Error	0.0000	9	0.0000			
Cor Total	2.100E+05	281				

++: Extremely significant (p-value<0.001); +: Significant (0.001<p-value<0.05); -: Insignificant (p-value>0.05)

$$COP = 200.412 - 12.0985t_1 - 276.63RH_1 - 1.49863v_1 + 3.74698t_2 + 95.4495RH_2 + 7.51686v_2 - 8700.1d + 9.99784H + 9.26987t_1RH_1 + 0.398513t_1v_1 - 0.0715521t_1t_2 - 1.30387t_1RH_2 - 0.713473t_1v_2 + 510.183t_1d - 3.51923RH_1t - 60.5629RH_1RH_2 - 3.37822RH_1v_2 + 8168.07RH_1d + 3.25294v_1v_2 + 735.308v_1d - 2.09248t_2RH_2 + 0.441354t_2v_2 - 346.909t_2d + 6.82876RH_2v_2 - 5970.39RH_2d - 2.67179v_2H + 2521.11dH + 0.176814t_1^2 + 112.344RH_1^2 - 4.05745v_1^2 - 2.24382v_2^2 - 7.42548H^2 \quad (22)$$

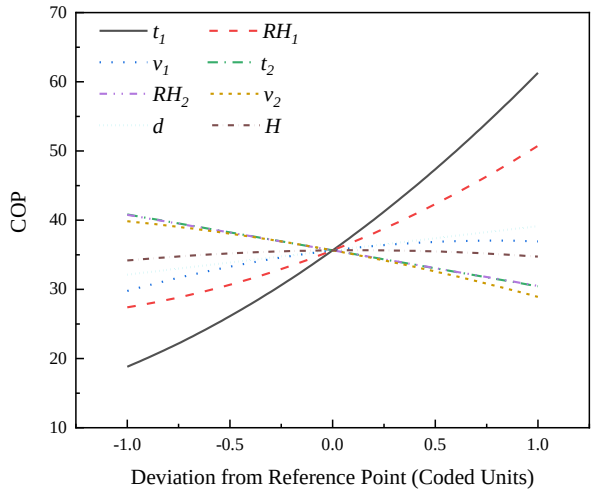

Fig. 15 Perturbation plot of COP

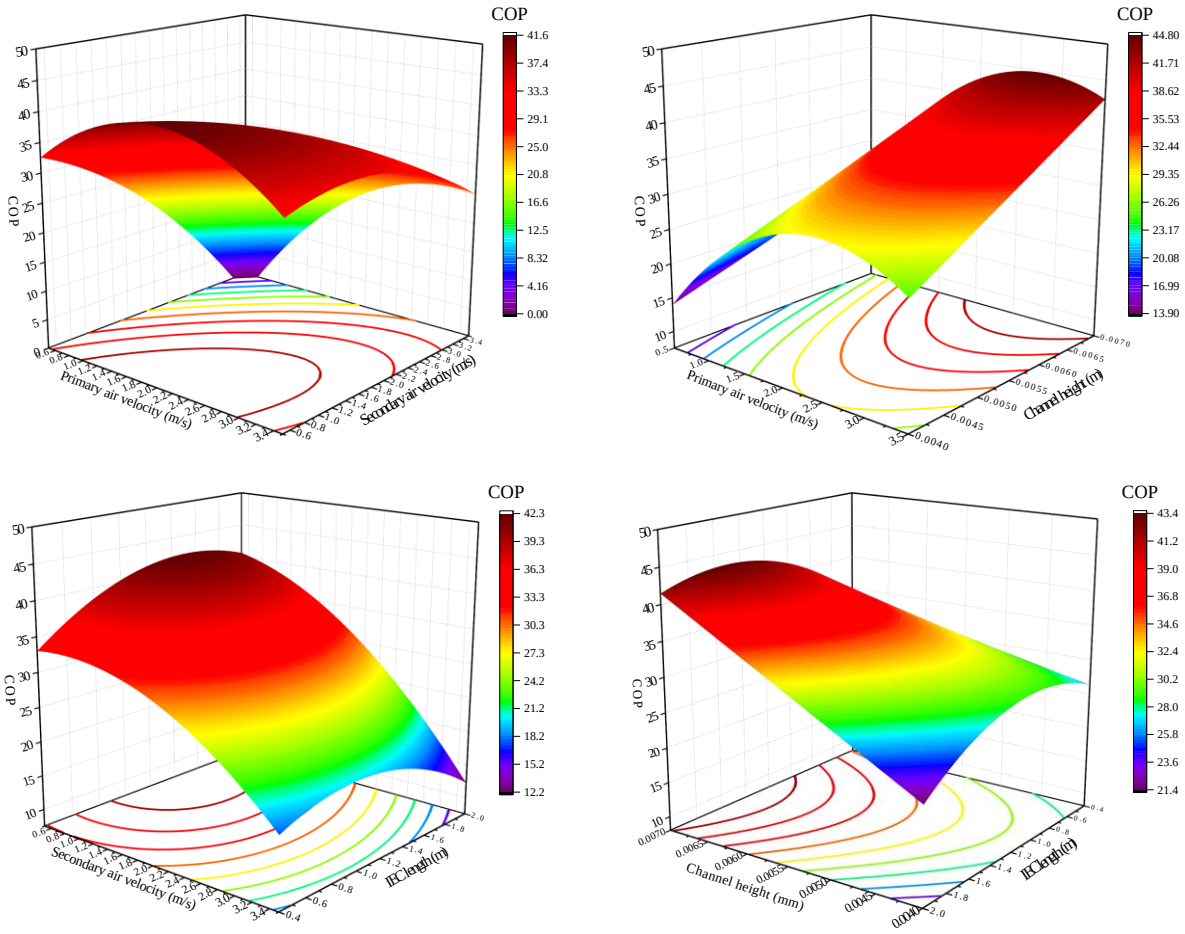

Fig. 16 The response surface and contour for the influence of factors on the COP (a) v_1~v_2 (b) v_1~d (c) v_2~H (d) d~H

The impact of the single factor on the response trend is shown in the perturbation plot. As shown in Fig. 15, the greater primary air inlet temperature ($t_{1,i}$), relative humidity ($RH_{1,i}$), velocity (v_1), channel height (d), and IEC height (H) are directly proportional to this output response. The curve of $t_{1,i}$ and $RH_{1,i}$ are steeper compared with the other three, indicating higher sensitivity of them. The slopes of the former two factors keep growing, while primary air velocity (v_1) generally becomes flat, which means that the *COP* cannot be endlessly enhanced by raising v_1. On the other hand, the greater secondary air inlet temperature ($t_{2,i}$), relative humidity ($RH_{2,i}$), and velocity (v_2) inversely influence the value of *COP*. The slopes of the former two keep stable, but the velocity slope is gradually higher.

Regarding the response surfaces and contours, there are four interactive terms (v_1v_2, v_1d, v_2H, dH) of the adjustable factors that need to be presented after passing the AIC and the p-value comparison. As exhibited in Fig. 16, similar to the discussion in the single factor, the response value cannot be unlimitedly improved just by changing the factors to maximum or minimum value based on the variation trends. In other words, reducing the primary air velocity (v_1) and raising the secondary air velocity (v_2) may suffer from a counterproductive impact, and extending the channel height (d) and IEC height (H) are not always effective. The greatest *COP* of 41.5 locates at the point where v_1 =0.5 m/s and v_2= 1.85 m/s (Fig. 16(a)), and the peak point in Fig. 16(b) occurs given the condition of v_1 = 2.73 m/s and d= 0.007 m. For the other two pairs of factors, the maximum *COP*s reach 44.8 and 43.3

when providing the input factors of 0.5 m/s, H= 1.74 m (Fig. 16(c)) and d= 0.007 m, H= 1.48 m (Fig. 16(d)), respectively.

3.4 Performance prediction in the real project

In order to evaluate the prediction performance of the regression models, a case study was conducted based on the on-site measurement results from morning to noon of a summer day in a demonstration project. A primary air unit combining a cross-flow IEC and a cooling coil was installed at the plant room of a governmental building in Hong Kong. The real photo of the IEC section used in the project is shown in Fig. 17. The specifications of the IEC and average operating conditions are: H = L = 0.6 m, d= 0.004 m; v_1= 2.63 m/s; v_2= 0.96 m/s; $t_{2,i}$= 22.14℃, $t_{2,i,wb}$= 18.63℃. As presented in Fig. 18, the outlet primary air temperature and outlet primary air humidity deviations are within ±3% and ±6% compared with the measured data, respectively, indicating that the regression models can be employed for performance forecasting of the cross-flow IEC.

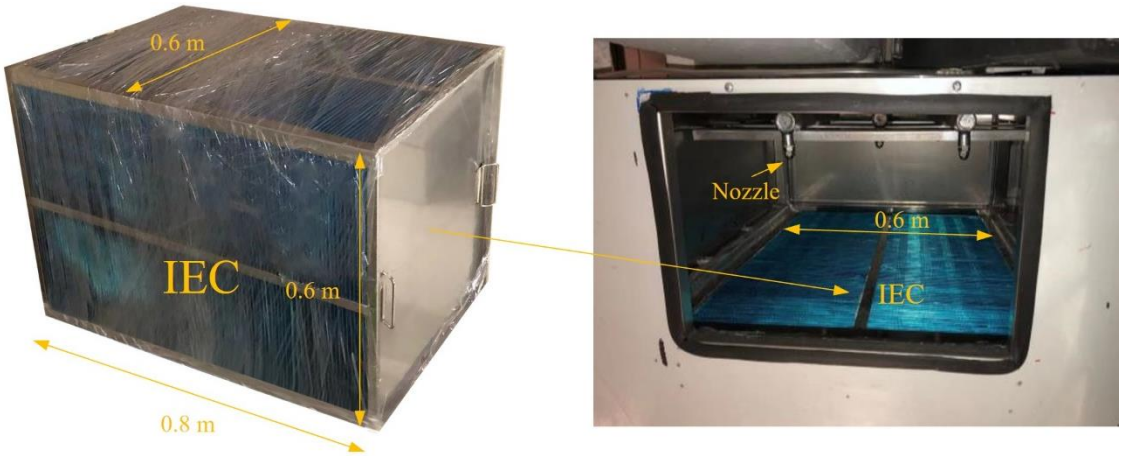

Fig. 17 Photo of the installed IEC and spraying nozzles

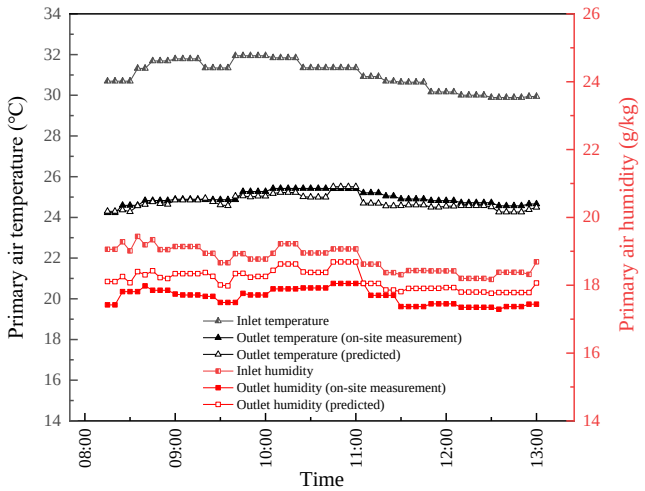

Fig. 18 Comparison between the results from the regression models and the on-site measurement data

3.5 Design optimization of the IEC

In addition to the forecasting purpose, the RSM-based model can be used to optimize the IEC during the design stage of the AC system. Normally, users expect higher wet-bulb efficiency, enlargement coefficient, and *COP* for greater cooling performance and higher energy efficiency. In practice, the primary air velocity (v_1) is usually larger than the secondary air speed (v_2) to maintain the positive pressure, and the indoor air temperature is often higher than 24℃. Therefore, multi-objective optimization can be conducted using the desirability function considering the above conditions. The related functions are shown from Eq. (23) to Eq. (25). The desirability is a value between 0 and 1, where 1 represents the ideal response, and 0 represents the worst response [43]. During the optimization process, wet-bulb efficiency, enlargement coefficient, and *COP* are given equal importance. Then, the desirability is maximized based on the multi-goals and the limited ranges of the input factors presented in Table 10, which can achieve the highest desirability of 0.787 among all solutions.

$$D = (d_1{}^{WF_1} d_2{}^{WF_2} \dots d_n{}^{WF_n})^{\frac{1}{\sum_1^n WF_n}} \tag{23}$$

When the goal is to maximize one response, Eq. (24) should be employed:

$$d = \begin{cases} 0, & (y \le l) \\ \left(\dfrac{y-l}{U-l}\right)^r, & l \le y \le U \\ 1, & (U \le y) \end{cases} \tag{24}$$

When the goal is to minimize one response, Eq. (25) is utilized:

$$d = \begin{cases} 1, & (U \le y) \\ \left(\dfrac{U-y}{U-l}\right)^r, & l \le y \le U \\ 1, & (y \le l) \end{cases} \tag{25}$$

Table 10 Optimized solution of the cross-flow IEC

Name	Goal	Lower Limit	Upper Limit	Solution
t_1	is in range	20	40	40
RH_1	is in range	30	1	84.6
v_1	is in range	1.6	3.5	1.60
t_2	is in range	24	27	25.81
RH_2	is in range	40	80	75.2
v_2	is in range	0.5	1.5	1.5
d	is in range	0.004	0.007	0.006
H	is in range	0.4	2	1.78
η_{wb}	maximize	0.37	1	0.68

ε	maximize	1	4.32	4.31
$t_{1,o}$	None	15.37	29.25	28.13
$w_{1,o}$	None	7.91	25.51	24
COP	maximize	3.7	116.3	116.3
			Desirability	0.787

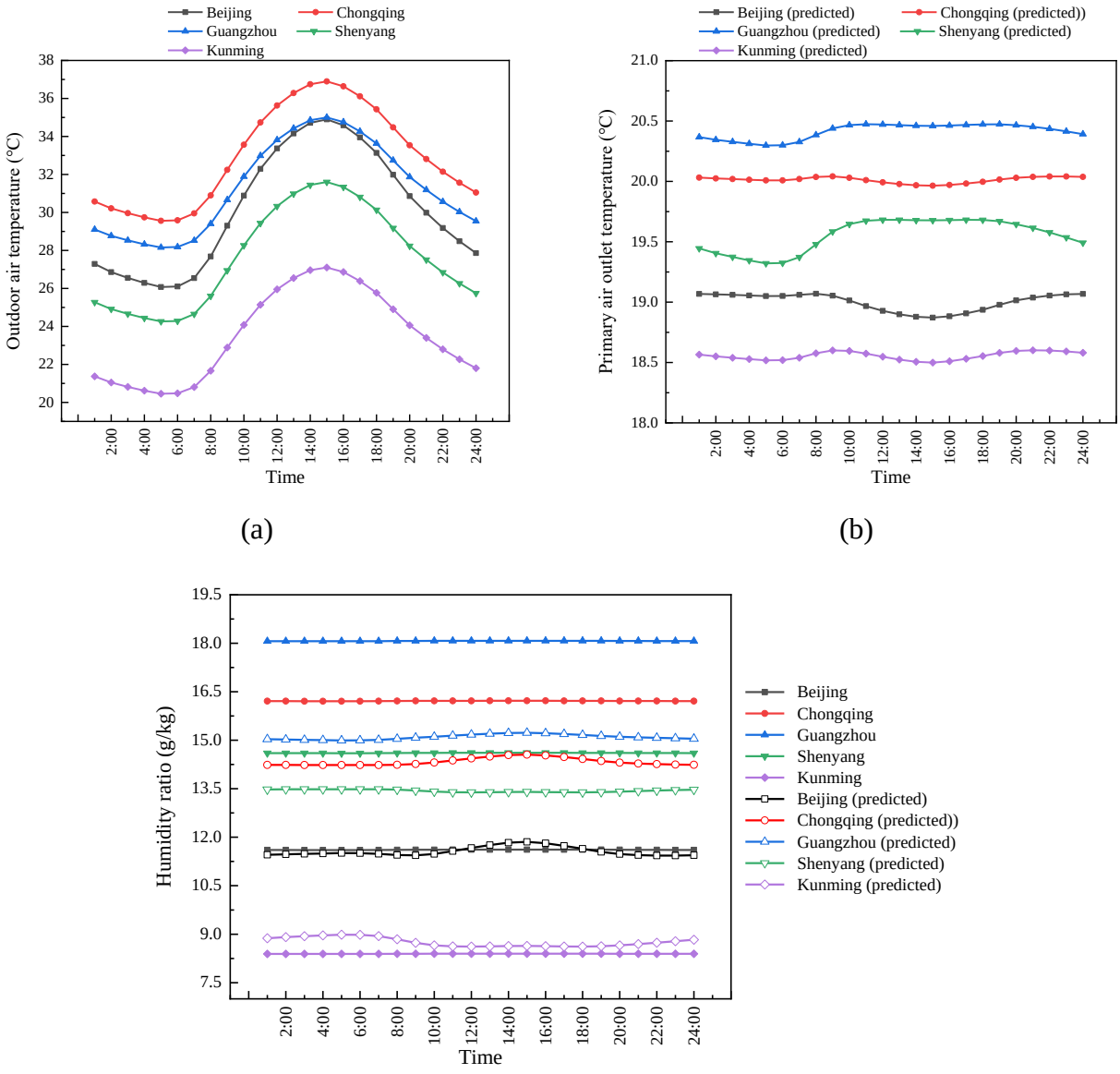

Fig. 19 Performance forecasting of the optimized IEC in five typical cities (a) Outdoor air temperature (b) Primary air outlet temperature (c) Outdoor air and primary air outlet humidity

Using the optimized factors, the performance of the IEC is predicted in five typical cities (Shenyang, Beijing, Chongqing, Kunming, and Guangzhou) with different climate conditions in China [9]. The weather information is obtained from the Energyplus official website [44], and the outdoor

weather conditions in the design day of each city are used for prediction. In the design stage, the controllable factors are the velocities (v_1 and v_2), the height of the IEC (H), and the channel height (d). The primary air inlet temperature ($t_{1,i}$) and humidity ratio ($w_{1,i}$) are calculated by inputting the optimized adjustable factors, the indoor air setpoint (25℃, 50% [45]), and the weather information in the summer design day. As shown in Fig. 19(a), Chongqing has the hottest dry-bulb air temperature, followed by Guangzhou and Beijing, while the outdoor air temperature in Kunming is much lower. Fig. 19(b) exhibits the predicted results from the regression model of temperature. The average temperature drop of 12.9℃ was most significant in Chongqing with the optimized IEC, and the values were also good in Beijing (11.1℃) and Guangzhou (10.9℃). In respect to the outdoor humidity ratio Fig. 19(c), Guangzhou, Chongqing, and Shenyang rank the first three. Condensation can be obviously observed in the three cities with average moisture content removal of 2.97 g/kg, 1.88 g/kg, and 1.17 g/kg, while the air dehumidification is much tiny in Beijing and Kunming due to the lower dewpoint temperature compared with the secondary air wet-bub temperature.

4. Conclusions

This study proposed the regression models of the cross-flow indirect evaporative cooler (IEC) using response surface methodology (RSM) for performance prediction in different weather conditions. Eight factors were determined as the inputs, and five indicators were selected as the output responses. The central composite design (CCD) was employed to generate the matrix for the RSM-based model, and the matrix response results originated from an established numerical IEC model validated by the experimental data. Then, the regression models were formulated, and the influences of the single and adjustable interactive factors on the output responses were analyzed. Besides, the developed models are assessed by comparing the forecasted values with the on-site measurement data in a real project. Finally, the multi-objective optimization is conducted with predicted IEC performances in five typical cities of China. The main findings are summarized as follows.

1) The sensitivity of the input factors changes in the different responses, but the primary air inlet temperature and relative humidity are always more sensitive compared with the other factors. Among the four adjustable factors, the channel height is relatively insensitive than the IEC height and the velocities of primary and secondary air, which can be considered as the last priority.

2) The response value cannot be unlimitedly improved by changing the single factors to maximum or minimum value based on the variation trends. The interactive factors need to be controlled simultaneously to get better performance. The adjustable factors can be determined as v_1 = 1.6 m/s, v_2= 1.5 m/s, d= 0.006, and H= 1.785 with the desirability of 0.787 considering the commonly-adopted ranges of input parameters after the multi-objective optimization.

3) The regression models are used to predict the IEC performance in cities with different climate regions. The optimized IEC is expected to achieve temperature drops of 12.9℃, 11.1℃, and 10.9℃ in Chongqing, Beijing, and Guangzhou, respectively. Regarding humidity prediction, noticeable condensation can be anticipated in Guangzhou, Chongqing, and Shenyang, while the possibility of air dehumidification is much slighter in the other two cities because of the low dewpoint temperature under their local weather conditions.

In summary, the regression models developed in this study can straightforwardly predict the IEC performance in different climate regions, which may help the engineering design and provide the guidance for the IEC optimization.

CRediT authorship contribution statement

Wenchao Shi: Conceptualization; Methodology; Program; On-site measurement; Formal analysis; Writing – original draft. **Hongxing Yang:** Conceptualization; Supervision; Funding acquisition; Writing – review & editing; **Xiaochen Ma:** Validation; Data curation; Resources; **Xiaohua Liu:** Writing – review & editing; Supervision.

Declaration of competing interest

The authors declare that they have no known competing financial interests or personal relationships that could have appeared to influence the work reported in this paper.

Acknowledgment

The authors wish to acknowledge the financial support provided by the General Research Fund projects of the Hong Kong Research Grant Council (Ref. No.: 15213219 and 15200420).

References

[1] J. Chen, Q. Gong, and L. Lu, "Evaluation of passive envelope systems with radiative sky cooling and thermally insulated glazing materials for cooling," *Journal of Cleaner Production,* vol. 398, p. 136607, 2023/04/20/ 2023.

[2] X. Liu, X. Liu, Y. Jiang, T. Zhang, and B. Hao, "PEDF (photovoltaics, energy storage, direct current, flexibility), a power distribution system of buildings for grid decarbonization: Definition, technology review, and application," *CSEE Journal of Power and Energy Systems,* pp. 1-18, 2022.

[3] A. Y. T. Al-Zubaydi and G. Hong, "Experimental study of a novel water-spraying configuration in indirect evaporative cooling," *Applied Thermal Engineering,* vol. 151, pp. 283-293, 2019/03/25/ 2019.

[4] Q. Chen *et al.*, "Experimental study of a sustainable cooling process hybridizing indirect evaporative cooling and mechanical vapor compression," *Energy Reports,* vol. 8, pp. 7945-7956, 2022/11/01/ 2022.

[5] X. Ma, W. Shi, and H. Yang, "Study on water spraying distribution to improve the energy recovery performance of indirect evaporative coolers with nozzle arrangement optimization," *Applied Energy,* vol. 318, 2022.

[6] S. Z. Shahvari, V. A. Kalkhorani, and J. D. Clark, "Performance evaluation of a metal organic frameworks based combined dehumidification and indirect evaporative cooling system in different climates," *International Journal of Refrigeration,* vol. 140, pp. 186-197, 2022/08/01/ 2022.

[7] X. Ma, W. Shi, and H. Yang, "Improving the performance of indirect evaporative cooler for energy recovery from the perspective of nozzle configuration: A CFD model analysis," *Journal of Building Engineering,* p. 107195, 2023/06/26/ 2023.

[8] H. Yang, W. Shi, Y. Chen, and Y. Min, "Research development of indirect evaporative cooling technology: An updated review," *Renewable and Sustainable Energy Reviews,* vol. 145, 2021.

[9] J. Wang, J. Lu, W. Li, C. Zeng, and F. Shi, "Numerical study on performance of a hybrid indirect evaporative cooling heat recovery heat pump ventilator as applied in different climatic regions of China," *Energy,* vol. 239, p. 122431, 2022/01/15/ 2022.

[10] M. W. Shahzad *et al.*, "A spatiotemporal indirect evaporative cooler enabled by transiently interceding water mist," *Energy,* vol. 217, p. 119352, 2021/02/15/ 2021.

[11] A. M. Blanco-Marigorta, A. Tejero-González, J. M. Rey-Hernández, E. Velasco Gómez, and R. Gaggioli, "Exergy analysis of two indirect evaporative cooling experimental prototypes," *Alexandria Engineering Journal,* vol. 61, no. 6, pp. 4359-4369, 2022/06/01/ 2022.

[12] Y. Zhou, Z. Yan, Q. Dai, and Y. Yu, "Experimental study on the performance of a novel hybrid indirect evaporative cooling/thermoelectric cooling system," *Building and environment,* vol. 207, p. 108539, 2022.

[13] U. Sajjad *et al.*, "A review of recent advances in indirect evaporative cooling technology," *International Communications in Heat and Mass Transfer,* vol. 122, p. 105140, 2021/03/01/ 2021.

[14] A. Adam, D. Han, W. He, and J. Chen, "Numerical analysis of cross-flow plate type indirect evaporative cooler: Modeling and parametric analysis," *Applied Thermal Engineering,* vol. 185,

p. 116379, 2021/02/25/ 2021.

[15] J. Lin, K. Thu, S. Karthik, M. W. Shahzad, R. Wang, and K. J. Chua, "Understanding the transient behavior of the dew point evaporative cooler from the first and second law of thermodynamics," *Energy Conversion and Management,* vol. 244, p. 114471, 2021/09/15/ 2021.

[16] I. Hussain *et al.*, "Evaluating the parameters affecting the direct and indirect evaporative cooling systems," *Engineering analysis with boundary elements,* vol. 145, pp. 211-223, 2022.

[17] S. Anisimov, D. Pandelidis, A. Jedlikowski, and V. Polushkin, "Performance investigation of a M (Maisotsenko)-cycle cross-flow heat exchanger used for indirect evaporative cooling," *Energy,* vol. 76, pp. 593-606, 2014/11/01/ 2014.

[18] W. Shi, Y. Min, X. Ma, Y. Chen, and H. Yang, "Dynamic performance evaluation of porous indirect evaporative cooling system with intermittent spraying strategies," *Applied Energy,* vol. 311, 2022.

[19] B. Zhou, J. Lv, M. Zhu, L. Wang, L. Liang, and Q. Chen, "Simulation study of a thin membrane inclined automatic wicking dew-point evaporative cooling device," *Journal of Building Engineering,* vol. 72, p. 106601, 2023/08/01/ 2023.

[20] A. Pacak, B. Baran, K. Sierpowski, Z. Malecha, and D. Pandelidis, "Application of computational fluid dynamics (CFD) methods to analyze energy efficiency of indirect evaporative coolers," *International Communications in Heat and Mass Transfer,* vol. 143, p. 106727, 2023/04/01/ 2023.

[21] Y. Zhang, H. Zhang, H. Yang, Y. Chen, and C. W. Leung, "Counter-crossflow indirect evaporative cooling-assisted liquid desiccant dehumidifier: Model development and parameter analysis," *Applied Thermal Engineering,* vol. 217, p. 119231, 2022/11/25/ 2022.

[22] D. Pandelidis *et al.*, "Performance analysis of rotary indirect evaporative air coolers," *Energy Conversion and Management,* vol. 244, p. 114514, 2021/09/15/ 2021.

[23] Y. Wan, Z. Huang, A. Soh, and K. Jon Chua, "On the performance study of a hybrid indirect evaporative cooling and latent-heat thermal energy storage system under commercial operating conditions," *Applied Thermal Engineering,* vol. 221, p. 119902, 2023/02/25/ 2023.

[24] H. Yan, Y. Chen, Y. Min, and Y. Pan, "An adaptive controller based dynamic simulation of household air-conditioner with indirect evaporative cooler as dedicated outdoor air system," *Energy and Buildings,* vol. 274, p. 112454, 2022/11/01/ 2022.

[25] Y. Min, Y. Chen, W. Shi, and H. Yang, "Applicability of indirect evaporative cooler for energy recovery in hot and humid areas: Comparison with heat recovery wheel," *Applied Energy,* vol. 287, 2021.

[26] W. Shi, Y. Min, Y. Chen, and H. Yang, "Development of a three-dimensional numerical model of indirect evaporative cooler incorporating with air dehumidification," *International Journal of Heat and Mass Transfer,* vol. 185, p. 122316, 2022/04/01/ 2022.

[27] S. Rasheed, M. Ali, H. Ali, and N. A. Sheikh, "Experimental evaluation of indirect evaporative cooler with improved heat and mass transfer," *Applied Thermal Engineering,* vol. 217, p. 119152, 2022/11/25/ 2022.

[28] S. De Antonellis, C. M. Joppolo, P. Liberati, S. Milani, and L. Molinaroli, "Experimental analysis of a cross flow indirect evaporative cooling system," *Energy and Buildings,* vol. 121,

pp. 130-138, 2016/06/01/ 2016.
[29] Y. Min, Y. Chen, and H. Yang, "A statistical modeling approach on the performance prediction of indirect evaporative cooling energy recovery systems," *Applied Energy,* vol. 255, p. 113832, 2019/12/01/ 2019.
[30] T. R. Kiran and S. P. S. Rajput, "An effectiveness model for an indirect evaporative cooling (IEC) system: Comparison of artificial neural networks (ANN), adaptive neuro-fuzzy inference system (ANFIS) and fuzzy inference system (FIS) approach," *Applied Soft Computing,* vol. 11, no. 4, pp. 3525-3533, 2011/06/01/ 2011.
[31] W. Shi, X. Ma, Y. Gu, Y. Min, and H. Yang, "Indirect evaporative cooling maps of China: Optimal and quick performance identification based on a data-driven model," *Energy Conversion and Management,* vol. 268, 2022.
[32] W. Yan, X. Meng, X. Cui, Y. Liu, Q. Chen, and L. Jin, "Evaporative cooling performance prediction and multi-objective optimization for hollow fiber membrane module using response surface methodology," *Applied Energy,* vol. 325, p. 119855, 2022/11/01/ 2022.
[33] T. Sun, T. Tang, C. Yang, W. Yan, X. Cui, and J. Chu, "Cooling performance and optimization of a tubular indirect evaporative cooler based on response surface methodology," *Energy and Buildings,* vol. 285, p. 112880, 2023/04/15/ 2023.
[34] A. Pakari and S. Ghani, "Regression models for performance prediction of counter flow dew point evaporative cooling systems," *Energy Conversion and Management,* vol. 185, pp. 562-573, 2019/04/01/ 2019.
[35] Y. Min, W. Shi, B. Shen, Y. Chen, and H. Yang, "Enhancing the cooling and dehumidification performance of indirect evaporative cooler by hydrophobic-coated primary air channels," *International Journal of Heat and Mass Transfer,* vol. 179, 2021.
[36] Y. Min, Y. Chen, and H. Yang, "Numerical study on indirect evaporative coolers considering condensation: A thorough comparison between cross flow and counter flow," *International Journal of Heat and Mass Transfer,* vol. 131, pp. 472-486, 2019/03/01/ 2019.
[37] B. Cheng and Y. Yao, "Design and optimization of a novel U-type vertical axis wind turbine with response surface and machine learning methodology," *Energy Conversion and Management,* vol. 273, p. 116409, 2022/12/01/ 2022.
[38] Y. Chen, H. Yang, and Y. Luo, "Indirect evaporative cooler considering condensation from primary air: Model development and parameter analysis," *Building and Environment,* vol. 95, pp. 330-345, 2016/01/01/ 2016.
[39] H. Zhang, H. Ma, S. Ma, and M. Yang, "Investigation on the performance of an indirect evaporative cooling system integrated with liquid dehumidification," *Energy and Buildings,* vol. 251, p. 111356, 2021/11/15/ 2021.
[40] D. Roy, S. Samanta, and S. Ghosh, "Performance optimization through response surface methodology of an integrated biomass gasification based combined heat and power plant employing solid oxide fuel cell and externally fired gas turbine," *Energy Conversion and Management,* vol. 222, p. 113182, 2020/10/15/ 2020.
[41] DesignExpert. (2023, 1st April). [Online]. Available: https://www.statease.com/software/design-expert/.
[42] M. Moradi, M. Fazlzadehdavil, M. Pirsaheb, Y. Mansouri, T. Khosravi, and K. Sharafi,

"Response surface methodology (RSM) and its application for optimization of ammonium ions removal from aqueous solutions by pumice as a natural and low cost adsorbent," *Archives of Environmental Protection,* vol. 42, no. 2, pp. 33-43, 2016.

[43] A. F. Boudjabi *et al.*, "Analysis and multi-response optimization of two dew point cooler configurations using the desirability function approach," *Energy Reports,* vol. 7, pp. 5289-5304, 2021/11/01/ 2021.

[44] EnergyPlus. (2nd April). *Weather Data* [Online]. Available: https://energyplus.net/weather.

[45] Q. Liu, C. Guo, X. Ma, Y. You, and Y. Li, "Experimental study on total heat transfer efficiency evaluation of an indirect evaporative cooler," *Applied Thermal Engineering,* vol. 174, 2020.